Water content and nature of solutes in shallow-mantle fluids from fluid inclusions

Water content and nature of solutes in shallow-mantle fluids from fluid inclusions

Maria Luce Frezzotti[1], Simona Ferrando[2], Francesca Tecce[3], Daniele Castelli[2]

[1]Department of Earth Sciences, University of Siena, Via Laterina 8, 53100 Siena, Italy.
marialuce.frezzotti@unisi.it; Tel. +39 0577 233929; Fax +39 0577 233938.

[2] Department of Earth Sciences, University of Torino, Via V. Caluso 35, 10125 Torino, Italy.
simona.ferrando@unito.it; daniele.castelli@unito.it

[3]IGAG – CNR, c/o Department of Earth Sciences, University of Rome "La Sapienza", P.za A. Moro 5, 00185 Roma, Italy. francesca.tecce@cnr.it

Abstract

This study discusses new and published data on the composition of fluid inclusions contained in mantle minerals of spinel and garnet peridotite xenoliths, in samples from geodynamically distinct settings (Ethiopian plateau, Hawaii, Canary Islands, and western Mediterranean region). Based on spectroscopic Raman and FTIR analyses we show that, contrary to a commonly held view, fluid inclusions either contain relevant amounts of unsuspected H_2O, or represent a "dehydrated" composition from multicomponent aqueo-carbonic fluids. We identify water loss from fluid inclusions through decrepitation, stretching and hydrogen diffusion. We also show that talc, magnesite, chlorides, and sulfates represent common phases in fluid inclusions. Talc and magnesite form through reactions of fluids with the surrounding minerals. Thermodynamic modeling in the MFSHC system of observed reactions between fluid inclusions and surrounding mantle minerals provides the basis for predicting water amounts in shallow-mantle fluids, and suggests X_{H2O} in the range of 10-50 mole %. Model hydrous fluids are relatively enriched solutions, dominated by Si, Cl, and alkalies, with significant Ca, and S, and low Mg and Fe. This study argues that multicomponent hydrous fluids may be widespread in the shallow mantle, not only in subduction zones but also in intraplate and extensional settings.

Keywords: Mantle petrology, Upper mantle fluid, fluid inclusions, Raman spectroscopy, FT-IR spectroscopy

Introduction

The volatile (e.g., C, O, H and halogens) inventory in the Earth's upper mantle includes accessory phases, nominally anhydrous minerals (NAMS), along with mobile fluid phases and volatile-rich melts (e.g., Bell et al., 2003; Bolfan-Casanova et al., 2000; Dasgupta and Hirschmann, 2006; Green and Falloon, 1998; Thompson, 1992; Wyllie and Ryabchikov, 2000). Hydrous fluids are critical to understand the structure and dynamics of the upper mantle, as they play a major role during deformation and recrystallization processes, and control partial melting of peridotites in upwelling mantle (Asimow and Langmuir, 2003; Dixon et al., 2004; Hirth and Kohlstedt, 2003; Katayama and Karato, 2008; Katz, et al., 2003). Furthermore, water has a major control on the oxidation state and on the selective enrichment in alkalies, large ion lithophile elements (LILE), and light rare earth elements (LREE) of mantle rocks (Bailey, 1982; Dixon et al., 2002; Kessel et al., 2005). Despite considerable progresses in modeling fluid behavior, our understanding of the exact nature and composition of hydrous mantle fluids is hampered by the absence of distinctive chemical signatures in many peridotites.

C-O-H fluid speciation is largely dependent on oxygen fugacity (fO_2). H_2O and CO_2 are predicted to be the major fluid components in the shallow mantle at $P \leq$ 2-3 GPa, for fO_2 equal to or greater than the quartz-fayalite-magnetite buffer (QFM) (Connolly, 1995; French, 1966; Huizenga, 2001, 2005; Ohmoto and Kerrick, 1977; Shi and Saxena, 1992; Zhang and Duan, 2009, 2010). Studies of gasses contained in or released from magmas, and of accessory mantle minerals (e.g., phlogopite, amphibole and apatite) suggest that fluids should contain CO_2, H_2O, and halogens (Marty and Tolstikhin, 1998; Marty and Zimmermann, 1999; Murck et al., 1978; Oppenheimer et al., 2011; O'Reilly and Griffin, 2000; Patino Douce et al., 2011; Smith et al., 1981; Wallace, 2003).

Fluid inclusions are the best natural samples to provide evidence for the nature of shallow-mantle fluids. However, we have known for a long time that fluid inclusions in peridotites are

typically CO_2-rich relative to other volatiles (cf. reviews by Andersen and Neumann, 2001; Pasteris, 1987; Roedder, 1965; 1984). This discrepancy between the fluid composition observed in inclusions and that predicted by oxy-thermobarometry has bolstered models that suggest any mobile hydrous component to be partitioned to melt phases, such as silicate and carbonate melts (e.g., Luth, 2003; Murck et al., 1978; Thompson, 1992). Consequently, the apparent absence of H_2O has undermined the credibility of fluid inclusions as tracers of mantle processes, and has brought some authors to propose that most fluid inclusions represent late features, mainly related to deep magma degassing during ascent of peridotite xenoliths (e.g., Pasteris, 1987).

A full survey of fluid inclusions in mantle rocks does not fit the view of "pure" CO_2 fluids well. For example, Andersen et al. (1984) first proposed CO_2-brine fluids in peridotites from extensional mantle settings based on the association of carbonate and chlorine-bearing amphibole in CO_2 inclusions in peridotites from Bullenmeri (SE Australia). Similarly, Frezzotti et al. (2002a, and b) suggested that aggregates of talc and NaCl lining CO_2 inclusion cavities in olivine from peridotite of Tenerife (Canary Islands) formed as the result of post-entrapment chemical reaction between CO_2-brine fluids and the surrounding minerals. Recently, H_2O has been detected in deep diamond-bearing CO_2-rich fluid inclusions in garnet pyroxenites from Oahu, Hawaii (Frezzotti and Peccerillo, 2007). In addition, brine inclusions have been described in peridotites from subduction-zone settings with increasing frequency (e.g., Hidas et al., 2010; McInnes et al., 2001; Scambelluri et al., 1997; Trial et al., 1984).

This study is aimed to check for the presence of water in fluid inclusions formed at mantle depths in several suites of metasomatized peridotite xenoliths from the Ethiopian plateau, Hawaii, and the western Mediterranean region, using Raman and Fourier transform infrared (FT-IR) microspectroscopies. We compare the present results with the results of previously published studies and critically reevaluate the composition of fluid phases at shallow-mantle depths. The present study documents that there is, or there was, a hydrous solute-rich hydrous component in

87 many mantle fluids trapped as inclusions. A thermodynamic model to evaluate the H_2O budget in
88 shallow-mantle fluids is proposed. Although the present study focuses on mantle rocks, our
89 approach is equally applicable to eclogites, migmatites, and granulites in the lower continental
90 crust, where hydrous fluids are often predicted but not observed in fluid inclusions (e.g.,
91 Hollister, 1990; Touret, 1981, 2001).

92

93 1. **Description of studied samples**

94

95 We have investigated fluid inclusions in several suites of metasomatized spinel and garnet
96 peridotite xenoliths. Rocks were selected from intraplate or extensional tectonic settings related
97 recent to Plio-Quaternary volcanism. Our goal was to focus on fluid inclusions formed at mantle
98 depths in order to study the composition of mobile mantle fluid phases. For this reason, we
99 selected those peridotites which did not show significant melt infiltration, and where fluid
100 inclusions did not contain glass (i.e., volatile-rich melts). Fluid inclusions were analyzed in
101 olivine, orthopyroxene and clinopyroxene. Studied peridotites and fluid inclusions are described
102 in the following paragraphs and presented in Table 1.
103 Six pargasite-bearing spinel lherzolites were selected from a suite of peridotites in Quaternary
104 basanitic lavas from a cinder cone located in the Lake Tana region, part of the Ethiopian Plateau
105 (Ferrando et al., 2008; Table 1). Rocks show protogranular to porphyroclastic textures and
106 equilibrated in the lithosphere at 950–1015 °C and 1.3–2.0 GPa (Ferrando et al., 2008).
107 Peridotites contain Cl-rich pargasite, and cryptic enrichments in Fe, Al, LILE and Pb are
108 observed in clinopyroxene (Frezzotti et al., 2010). Coeval CO_2-rich fluid inclusions tiny (5–30
109 μm) occur in olivine and orthopyroxene porphyroclasts and subordinately in clinopyroxene,
110 along short intragranular trails. Orthopyroxene is rich in fluid inclusions and preserves the
111 highest density fluids (Table 1). Liquid water was detected in three CO_2-rich inclusions in

orthopyroxene and olivine under the microscope and the heating-freezing stage. From these observations, the estimated fluid composition is X_{CO2} = 0.64, X_{H2O} = 0.33, X_{Na} = 0.006, X_{Mg} = 0.006, X_{Cl} = 0.018, and the calculated isochores indicate trapping pressures, *P*, of 1.4-1.5 GPa, at 950 °C (Table 1). Modeled fluid composition is in agreement with the formation of Cl-rich metasomatic hydrous phases and with metasomatic enrichments in clinopyroxenes (Frezzotti et al., 2010). High Cl, LILE, and Pb in model metasomatic fluid phases point to a contribution of recycled altered oceanic lithosphere component in their source.

Four garnet pyroxenite samples were borrowed from the Jackson collection (Jackson and Wright, 1970) of the National Museum of Natural History (Washington D.C., USA). These are from alkali-post erosional stage Honolulu volcanics (< 1 m.y.) at Salt Lake Crater (SLC), Koolau shield, in the Island of Oahu, Hawaii (Clague and Frey, 1982; Lassiter at al., 2000; Sen, 1988). SLC garnet pyroxenites show coarse granular textures and consist of clinopyroxene (diopside-augite; > 60 % vol), olivine, orthopyroxene, garnet, and spinel. Garnet is of secondary origin, and mainly formed through exsolution from pyroxene during recrystallization processes. Although amphibole and phlogopite were previously reported (cf., Sen, 1988), traces of phlogopite were observed only in one sample. SLC garnet pyroxenites were interpreted as crystal cumulates from the recent Hawaiian volcanism in the Pacific lithosphere (*P* = 1.6-2.2 GPa). Recent reports of majoritic garnet and of microdiamonds imply a much deeper origin (ca. 4.5-5 GPa; Frezzotti and Peccerillo, 2007; Keshav and Sen, 2001, 2003; Keshav et al., 2007; Wirth and Rocholl, 2003). According to Keshav et al. (2007), garnet pyroxenites represent high-pressure cumulates related to polybaric magma fractionation in the asthenosphere. Early high-density to superdense CO_2 (d = 1.16-1.21 g/cm^3) fluid inclusions (≤ 5–6 μm) occur in clinopyroxene and subordinately in orthopyroxene, generally distributed along (010) directions. Superdense CO_2 is recognized by initial melting at the temperature of partial homogenization to liquid (-56.6°C; ThLs); final melting (TsL) occurs at temperatures up to - 50.8°C (Table 1; Frezzotti et al., 1992). Early inclusions contain microdiamonds and traces of H_2O, N_2 and H_2S

(Frezzotti and Peccerillo, 2007), but no glass/melt. Rare carbonate inclusions, and mixed CO_2 + carbonate ± diamond inclusions have also been observed. These characteristics are consistent with a genetic link of fluids with ephemeral carbonate-rich melt generated in the asthenosphere within the diamond stability field (Frezzotti and Peccerillo, 2007).

Four spinel phlogopite-harzburgites and one dunite from central Italy occur in lamproitic lavas of Torre Alfina volcano (0.9-0.8 M.y.; Conticelli and Peccerillo 1990). Xenoliths consist of olivine and subordinate (3–12 vol. %) orthopyroxene porphyroclasts showing protogranular textures (Table 1). Rare anhedral clinopyroxene occurs in the interstices between deformed olivines. Brownish to black spinels are also present as isolated coarse crystals (> 1 mm) or as smaller grains. Metasomatic phlogopite is present in amounts variable from less than 1 up to 10% of the rock by mode. This has Sr-Nd ($^{87}Sr/^{86}Sr$ ~ 0.716 - 0.717; $^{143}Nd/^{144}Nd$ ~ 0.5121) isotopic signatures close to those of the host lamproites (Conticelli, 1998). Geothermobarometric studies indicate equilibrium pressures, *P*, of ca. 1.2-1.6 GPa, corresponding to a depth of 50 to 60 km, and temperatures, *T*, of 950–1080 °C (Pera et al., 2003; unpublished data). Rare CO_2-rich fluid inclusions are observed only in a few orthopyroxene porhyroclasts. Inclusions are tiny (≤ 5 μm) and distributed along (010) directions.

Mantle melting and generation of lamproites took place during opening of Western Mediterranean basins, after the Europe-Africa continental collision. Central Italian peridotites represent samples of a "hot" lithosphere, located close to the asthenosphere-lithosphere boundary (Frezzotti et al., 2009). Metasomatism involved the presence of subducted fluids/melts of continental origin related to older subduction events of Alpine age (Peccerillo, 2005, and references therein).

Three spinel dunites and two spinel pyroxenites from Sardinia are from the spatter cone of Monte Lisiri volcano (~0.9-0.1 Ma; Lustrino et al., 2000), near the village of Ittireddu in the Logudoro region, which is part of the recent Plio-Pleistocene anorogenic alkaline mafic volcanism in northern Sardinia. Dunites show porphyroclastic textures and consist mostly of olivine porphyroclasts, with very subordinate orthopyroxene and undeformed interstitial clinopyroxene

grains. Granular pyroxenites are dominated by clinopyroxene (> 85 vol. %), with subordinate olivine and orthopyroxene. Mineral thermometry indicates relatively low temperatures (950°C). In pyroxenites, modal metasomatism is testified by the presence of phlogopite (1-2 vol. %) with high Cl contents (ca. 0.4-0.5 wt %). In dunites and pyroxenites, intragranular trails of CO_2-rich fluid inclusions tiny (5–20 μm) are abundant in orthopyroxene and clinopyroxene, the highest CO_2 densities being recorded in clinopyroxene (Table 1). In Sardinia, the origin of pyroxenites has been related to deep cumulus processes, whereas peridotites have been interpreted as upper mantle residues variably affected by metasomatic processes by melts derived from partial melting of lower crustal rocks (Lustrino et al., 2000; 2004). Peccerillo (2005), however, did not exclude that metasomatism of the lithosphere beneath northern Sardinia might have occurred by subduction-related fluids or melts in Oligo-Miocene times, based on composition of mafic rocks.

Among selected samples, pyrope garnet is present only in Hawaiian pyroxenites, and it does not contain mantle fluid inclusions. In order to study the post-entrapment evolution of fluid inclusions in garnet, we additionally included one sample of whiteschist from the Dora Maira Massif in western Alps (Italy), a slice of continental crust that experienced subduction to ultra-high pressure conditions (P= 3.5 GPa, T= 750°C) (e.g., Ferrando et al., 2009, and references therein). Abundant aqueous fluid inclusions have been previously described in pyrope from these lithologies (Ferrando et al., 2009; Philippot and Selverstone, 1991).

2. **Analytical Methods**

Raman spectra of minerals and fluid inclusions containing C and H were acquired with a Labram microspectrometer (HORIBA Jobin Yvon) at the University of Siena. A polarized 514.5 nm water-cooled Ar-ion laser was used as the excitation source. The measured laser power was 300-500 mW at the source, and about 80% less at the sample surface. Raman spectra were collected through an OLYMPUS 100x objective (0.9 numerical aperture: excitation spot 1x1x5

190 µm in volume) for an acquisition time variable from 30 s to 180 s for each spectrum, and 1 to 10
191 accumulations. The slit width was set at 100 µm, and the corresponding spectral resolution was
192 1.5 cm^{-1}. Frequency wavenumbers of the Raman modes in the region 0-1800 cm^{-1} were
193 calibrated daily by the position of the diamond peak at 1331.7 cm^{-1}. Peak assignment of solid,
194 gaseous, and liquid phases was done by comparison with our reference library and database of
195 Raman spectra (http://www.dst.unisi.it/geofluids/raman/spectrum_frame.htm; Frezzotti et al.,
196 2012).

197 Morphological and chemical analyses of mineral phases in open fluid inclusions were
198 performed through scanning electron microscopy (SEM; Philips XL30) at the University of
199 Siena. This instrument is equipped with an energy-dispersive spectrometer (EDS-Philips EDAX
200 DX4). Selected doubly polished sections containing fluid inclusions were broken after
201 immersion in liquid nitrogen. Broken samples were immediately mounted on stubs and carbon
202 coated. Operating conditions were as follows: accelerating voltage 20 kV, beam current 23-25
203 µA, working distance 10-12 mm. Element maps with the theoretical inner pattern were obtained
204 using the ZAF method of correction. Natural silicates and oxides have been used as standards.

205 To reveal water diffusion from fluid inclusions into the structure of surrounding minerals,
206 we mapped the distribution -and concentrations of structurally -bound hydrogen in nominally
207 anhydrous minerals by synchrotron based FT-IR microspectroscopy. We selected those mantle
208 minerals where liquid H_2O was proven in fluid inclusions: olivine and pyroxenes from Ethiopian
209 peridotite xenoliths (Frezzotti et al., 2010), and garnet from Dora Maira whiteschists (Ferrando
210 et al., 2009). Analyses were performed by Fourier transform infrared (FT-IR) microspectroscopy
211 at the infrared beam-line SISSI (Source for Imaging and Spectroscopic Studies in the Infrared)
212 operating at the synchrotron laboratory ELETTRA in Trieste. Spectra were collected on a FTIR
213 spectrometer (Bruker IFS66/v) fitted with a Hyperion IR microscopy with a liquid-nitrogen-
214 cooled HgCdTe (MCT) detector. Infrared microscopy was performed on an infrared microscopy
215 system (Bruker) with a 16× magnification infrared objective. Spectra were collected at resolution

Formatted: Default Paragraph Font, Font: Calibri, 11 pt, Italian (Italy)

of 4 cm^{-1} and signal averaged for 128 scans on each data collection. Background spectra were recorded in air. For IR imaging studies, we used double-polished thick sections of xenoliths of known thickness. The spectral images were collected scanning areas of variable sizes (200-450 µm-long and 200-450 µm-wide), following a regular grid of square-aperture dimension of 20 µm equidistant by 20 µm in both directions (i.e., totals of 100-400 spectra), using a computer-controlled automated X-Y mapping stage. Interpretation of unpolarized spectra of H_2O followed the classical group frequency approach in which absorption bands are assigned to specific vibrational modes. OH concentrations in mineral phases were estimated from the integrated absorbance using the Beer-Lambert law (Paterson, 1982). Experimentally determined calibration constants for orthopyroxene are from Bell et al. (1995), and for olivine are from Bell et al. (2003). Since unpolarized FT-IR H_2O measurements are affected by large errors (30-50 %; cf., Demouchy et al., 2006), and imaging revealed H variations with position within single minerals, measured water contents are reported in intervals of tens of ppm, emphasizing the relative variations with distribution within single grains. Note that, liquid H_2O and/or hydrous minerals in fluid inclusions were also suggested by FT-IR absorption bands. However, spectra are not reported in the present paper, since we consider FT-IR microspectroscopy a less reliable diagnostic technique than Raman, because of its poorer resolution, and absence of confocality.

Petrogenetic grids were calculated in the MgO-FeO-SiO_2-H_2O-CO_2 (MFSHC) model system using the thermodynamic approach of Connolly (1990) and the internally consistent thermodynamic data set and equation of state for H_2O-CO_2 of Holland and Powell (2011), modified considering a typical mantle #mg [$Mg/(Mg+Fe^{2+})$ = 0.9] for olivine and orthopyroxene.

242 3. **Results**

243

244 Water in CO_2-rich fluid inclusions is traditionally revealed by optical studies, although
245 identification may be difficult in dense and often colored mantle minerals (cf., Roedder, 1972).
246 Water can be detected simply by using Raman and FT-IR spectroscopic techniques (cf., Frezzotti
247 and Peccerillo, 2007; Hidas et al., 2010; McMillan et al., 1996, and references therein). Results
248 are given in Table 2 and discussed in the following sections. Note that the potential of Raman
249 microspectroscopy for identifying water in mantle fluid inclusions has been known since the 80's
250 (e.g., Pasteris and Wanamaker, 1988). However, researchers failed to detect H_2O in fluid
251 inclusions at that time, probably because of the non-confocality and lower sensitivity of old
252 instruments.

253 *4.1 Uncovering aqueous fluids inside inclusions: Raman spectroscopy and EDAX-EDS analyses*

254 In almost all studied fluid inclusions H_2O in not visible. One exception is represented by a
255 few relatively-large fluid inclusions (> 20 – 30 μm) in orthopyroxene of spinel lherzolites from
256 the Ethiopian plateau, where thin (≤ 1 μm) liquid water films were recognized. In these
257 inclusions, presence of H_2O was confirmed by clathrates melting during microthermometric
258 studies at low temperatures (Table 2).

259 Raman microspectroscopy revealed the presence of liquid water in a minority of optically
260 "pure" CO_2 fluid inclusions (10-30 μm in size), for which pyroxenes were the enclosing
261 minerals, and a hydrous nature was recognized for the host mantle peridotites (e.g., Ethiopian
262 plateau and Central Italy; Table 2 and Fig. 1a). For example, a Raman spectrum of liquid H_2O is
263 reported in Figure 1b. The characterizing feature consists of a broad band centered
264 approximately at 3400-3450 cm^{-1} in the OH stretching region from 2900 to 3800 cm^{-1}. In those
265 fluid inclusions of less than 5 μm in size, a water film rimming the CO_2 does not generate a
266 discernible liquid H_2O Raman spectrum. However, Raman detection of H_2O was possible also in

these cases by spectra of isolated H_2O molecules dissolved in the CO_2 fluid (Table 2; Frezzotti and Peccerillo, 2007).

A coat of hydrous silicates and/or carbonates distributed along the rims of fluid inclusions was more commonly identified in place of molecular H_2O (Table 2; Fig 2 a-d). Talc (Tlc) was recognized by its band distribution in the OH^- region at 3677 cm^{-1} (Fig. 2f). More rarely, band distribution at 3450, 3638, 3673 cm^{-1} was observed, which corresponds to Mg-chlorite ($Mg_5AlSi_3AlO_{10}(OH)_8$; not shown). Magnesite (Mgs) was identified by its diagnostic Raman modes at 1092, 738, and 328 cm^{-1} (Fig. 2e). Whereas the presence of carbonates in fluid inclusions was revealed by optical microscopy (Fig. 2c and d), talc and chlorite were generally overlooked. The type and amount of minerals lining CO_2-rich inclusions depend mainly on the nature of the surrounding mineral (Table 2). In olivine, hydrous silicates and carbonates are common phases (Fig. 2b and c), and in a few cases completely fill the inclusions, without any fluid left (Fig. 2d). Conversely, in orthopyroxene and clinopyroxene, while carbonates are common, hydrous silicate minerals are less frequent (Fig. 2a).

Morphological observations by SEM images inside opened fluid inclusions showed that talc is constituted by very fine flakes, forming micrometer-sized packages distributed parallel to the enclosing mineral phase along the inclusions cavity walls (Fig. 3a and b). Talc and magnesite are often glazed by a thin coating, probably precipitated during opening of fluid inclusions (Fig. 3b). SEM-EDAX spectra indicate that the coating consists of Ca, Cl, S, K, and minor Si, Na, Al and Fe (Fig. 3c). Ca and S correspond to gypsum (Raman analysis, Fig. 3d and e). Other elements suggest the presence of KCl, NaCl, and probably SiO_2 and Fe-Al oxides (Fig. 3c-e).

In clinopyroxene from hydrous peridotites (Table 1), EDS-EDAX analyses showed that CO_2-rich inclusions occur in contact with a euhedral hydrous mineral, similar in size and chemically identical to the metasomatic phase present in the rocks: pargasite in peridotites from the Ethiopian plateau (Fig. 4a and c), and phlogopite in peridotites from Sardinia (Italy) (Fig. 4b and d).

293

294 *4.2 Mapping water diffusion from fluid inclusions: FT-IR spectroscopy*

295 Mapped hydrogen gradients in olivine, orthopyroxene and garnet revealed the change from
296 molecular water in the fluid inclusions to OH^- bonds in the surrounding anhydrous minerals.
297 Figure 5 reports the FT-IR synchrotron map of orthopyroxene and garnet hosting several fluid
298 inclusion trails (f.i. in Fig. 5a and c). In orthopyroxene, the mapped sample area is 450x450 μm
299 (for a total of 180 spectra), and the x-y spatial resolution is 20x20 μm (on the order of the
300 inclusion size). The FT-IR map in Fig. 5b clearly shows an exponential increase of bonded
301 hydrogen approaching the inclusion region. The increase of hydrogen content is evident from
302 symmetrical differently colored haloes in orthopyroxene: calculated H_2O contents range from
303 about 50-100 ppm far from fluid inclusions (more than 100 μm) to about 400-600 ppm, close to
304 fluid inclusions. In garnet (mapped area 400x400 μm; x-y resolution 20x20 μm), we observed a
305 four- to fivefold enrichment of water in areas close to fluid inclusions (Fig. 5d). Hydrogen
306 gradients recorded by map contours represent actual water content variations in garnet with the
307 exception of the fluid inclusion trail area where water contents above 180-200 ppm in part result
308 from a contribution of molecular H_2O from the inclusions (red to pink areas in Fig. 5d).
309 In olivine (Fig. 6a; mapped area 280x280 μm; x-y resolution 20x20 μm), water enrichment is
310 less significant than in orthopyroxene and garnet. FT-IR maps in figures 6b and c show the
311 distribution of OH^- absorption bands in two separate regions: 3000-3600 cm^{-1} corresponding to
312 OH^- in olivine (Fig. 6b), and 3600-3800 cm^{-1} corresponding to OH^- in serpentine or talc (Fig. 6c;
313 Khisina et al., 2001). The distribution of the strongest absorbance peak of water migration points
314 to hydrogen diffusion from single fluid inclusions into the surrounding olivine. Presence of talc
315 or serpentine close to fluid inclusion trails further suggest that hydration reactions occurred not
316 only inside fluid inclusions but also in surrounding olivine (Fig. 6b).
317 In clinopyroxene, water enrichments close to fluid inclusion trails were not observed.
318

5 Discussion

5.1 There was water in fluid inclusions formed at shallow-mantle depths

The present study highlights significant dehydration of shallow-mantle fluids after trapping as inclusions. Diffusive loss of H_2O due to re-equilibration between the inclusion and host is demonstrated by the strong FT-IR absorbance peak of water migration in the host nominally anhydrous mantle minerals. Transport of water could have occurred under conditions of differential pressures and fluid fugacity at high *P* and *T* through lattice defects and microfractures. A high-concentration of dislocations around fluid inclusions was previously reported in olivine from Canary Islands peridotites, and was proposed to be the main mechanism for molecular fluid loss (Viti and Frezzotti, 2000; 2001). This diffusion-scenario is conceivable considering the extremely fast diffusion of H in olivine (Mackwell and Kohlstedt, 1990), and reinforces models proposed for selective H_2O loss from CO_2-H_2O inclusions in quartz (Bakker and Jansen, 1991; Romer et al., 2006; Sterner and Bodnar, 1989; Watson and Brenan, 1987).

Further, dehydration of mantle fluids is induced by reactions between residual H_2O fluids in the inclusions and the surrounding minerals. In magnesian olivine, the association of talc and magnesite may form at low *T* and *P* through the following reaction:

$$4Mg_2SiO_4 + H_2O + 5CO_2 = Mg_3Si_4O_{10}(OH)_2 + 5MgCO_3 \quad (1)$$

However, talc and magnesite relative volumes observed in fluid inclusions (Fig. 3a) suggest that sub-equal molar amounts of these two phases were produced during the reaction, given that the molecular weight of talc is about five times that of magnesite (379 vs. 84), for similar densities (2.78 vs. 3.01 g/cm^3). Relative proportions of talc and magnesite can be greatly modified if H_2O-CO_2 fluids contained SiO_2 in solution:

$$2Mg_2SiO_4 + H_2O + CO_2 + 2SiO_2(aq) = Mg_3Si_4O_{10}(OH)_2 + MgCO_3 \quad (2)$$

In magnesian orthopyroxene, formation of talc and magnesite can be described by a reaction:

344 $4MgSiO_3 + H_2O + CO_2 = Mg_3Si_4O_{10}(OH)_2 + MgCO_3$ (3)

345
346 However, while magnesite represents a common phase in fluid inclusions, talc is more rare.
347 It is thus possible that a second reaction such as:

348
349 $MgSiO_3 + CO_2 = MgCO_3 + SiO_2$ (4)

350
351 might have occurred between H_2O-CO_2 fluids of variable X_{H2O} and surrounding orthopyroxene.
352 In contrast, fluid inclusions in clinopyroxene do not seem to contain or have contained H_2O.
353 Talc and magnesite are rare, and FT-IR absorption maps do not show significant water
354 enrichments. This result is surprising, given that the capacity of clinopyroxene to store H_2O
355 greatly exceeds that of olivine at upper mantle pressures (Aubaud et al, 2004). Although we may
356 have overlooked some processes, as the studied clinopyroxene is from hydrous peridotites where
357 metasomatic amphibole or phlogopite are present, our preferred explanation for the analytical
358 data is that reaction of the hydrous fluid occurred along microfractures at the infiltration stage,
359 prior to inclusion formation. Hydration of clinopyroxene during microfracture healing is
360 suggested by formation of tiny pargasite (or phlogopite) grains, occurring with CO_2 fluid
361 inclusions along the same microfracture (Fig. 4). In olivine and orthopyroxene, similar hydration
362 reactions are inhibited, since they occur at lower temperatures below most mantle geotherms (see
363 also section 5.2), and hydrous mantle fluids are trapped inside inclusions. Interestingly, Lamb et
364 al. (1987) proposed a similar evolution to explain selective CO_2 enrichments observed in fluid
365 inclusions of some high-grade metamorphic rocks.

366

367 *5.2 Amounts of water in shallow-mantle fluids*

368 A critical question to petrological and geophysical studies is how much water was originally
369 present in shallow-mantle fluids. This issue can be investigated by modeling the reactions
370 between H_2O-CO_2 fluid inclusions and surrounding magnesian orthopyroxene (Mg/Mg+Fe=0.9)

371 in peridotites. For magnesian olivine, similar reactions cannot be modeled since they require
372 SiO_2 in the fluid (cf., reaction 2 in 5.1). Figure 7 shows *T*-X_{H2O} phase diagrams for the MFSHC
373 model system at different pressures. The model reactions can be used to simulate the chemical
374 re-equilibrations between aqueous-carbonic fluids with different X_{H2O} in inclusions and
375 surrounding orthopyroxene. These diagrams show that the minimum X_{H2O} necessary to induce
376 hydration reactions between fluid inclusions and surrounding minerals increases with increasing
377 fluid pressure. If we consider the formation of talc inside a fluid inclusion in orthopyroxene, at 1
378 GPa, the minimum X_{H2O} is 0.25 (see invariant point 1 in Fig. 7b), while at 0.5 GPa, it decreases
379 to X_{H2O} =0.1 (invariant point 1 in Fig. 7c). The maximum X_{H2O} should not exceed 0.5 regardless
380 of pressure, since ensuing reactions would consume equal amounts of H_2O and CO_2, whereas
381 observed fluid inclusions have CO_2-rich compositions. From figure 7, it is also evident that
382 reactions between H_2O-CO_2 fluid inclusions and the surrounding minerals cannot be a mantle
383 process, as talc and/or magnesite only forms as temperatures decrease below about 700-600°C
384 for variable pressures. We propose that eruption provides the conditions to induce reactions. In
385 explosive eruptions, temperatures of xenoliths fall below 600°C over 5-10 sec. of ballistic
386 transport through the air (Shaw, 2009). Even in slower-cooling lavas, xenoliths take only a few
387 hours to reach the same temperatures.

388 A strong dependency on pressure for hydrous fluid inclusion evolution is illustrated in Figure
389 8. Consider a dense CO_2-H_2O fluid inclusion with X_{H2O}=0.3 in orthopyroxene formed at 1.5 GPa
390 and 1000°C in a mantle peridotite. When this inclusion ascends rapidly and adiabatically in a
391 xenolith within the host magma, it will effectively become overpressurized (path a in Fig. 8). If
392 decrepitation does not occur, it arrives at the surface, and subsequent syn-, and post-eruptive
393 decrease of temperature will cool the fluid in the inclusion along an isochore (path b in Fig. 8).
394 At temperatures below approximately 700°C, CO_2-H_2O fluid reaction with surrounding minerals
395 promotes the formation of magnesite in inclusions, but not hydrous phases (i.e., reaction 4 in
396 5.1). As far as a fluid inclusion remains overpressurized during adiabatic ascent and cooling,

hydrous phases cannot form. When the same fluid inclusion decrepitates during ascent, so that fluid density resets to a lower value corresponding, for example, to $P < 1$GPa (below point 1 in Fig. 8), syneruptive cooling along isochore (path c in Fig. 8) would make the CO_2-H_2O fluids in the inclusion to react to form talc + magnesite (reaction 3 in 5.1).

In summary, thermodynamic modeling suggests that up to 50 mole % water should have been present in fluid inclusions formed at mantle depths in order to drive the observed reactions in orthopyroxene. Petrogenetic grids also show that syneruptive cooling in host peridotite xenoliths promotes fluid reactions with surrounding minerals. Lower overpressures in the fluid inclusion require a lower minimum water amount in the fluid in order for hydration reactions to take place. It appears reasonable to conclude that hydration reactions associated with diffusive water loss reset fluid inclusions to the minimum concentration of H_2O and produce a dehydration trend which may result in the "pure CO_2" inclusions often described in mantle minerals. It is noteworthy to recall that any geobarometric data derived from similar CO_2-rich inclusions could result in underestimates, since CO_2-rich fluids would have residual composition and density considerably lower than that of the original mantle fluids at the time of entrapment.

5.3 Reevaluation of shallow-mantle fluid composition

In the absence of pristine inclusions in mantle minerals, an accurate characterization of the chemistry of the aqueous fluid component is complicated. Even so, the identity of minerals precipitating inside fluid inclusions through reactions with surrounding minerals gives information on the nature of species in solution. Ubiquitous talc forming through fluid reaction with surrounding host phases indicates Si as a major solute component (cf., reactions 2 and 3 in 5.1). Additionally, relevant amounts of Cl, S, Ca, K, and Na are revealed by chlorides and gypsum precipitated in inclusions on cooling. Interestingly, K seems to be present in relatively higher amounts than Na. Sulfur has been identified either as hydrogen sulfide gas (H_2S), elemental sulfur (S_8), or as sulfate ions (hydrated form of SO_3) (Table1) depending on the

oxidation state of the fluid, and indeed sulfur appears to bear a major control over the oxidation state. The sulfate ions detected in some fluid inclusions are a real feature, since, eventual postentrapment fluid inclusion redox-reactions would tend to reduce sulfur (Grishina et al., 1992).

The model composition of saline multicomponent mantle fluids that emerges from the present study is in agreement with formation of Cl-rich hydrous metasomatic phases and with extreme LILE enrichments in the studied peridotites (cf., section 2). In addition, the applicability of new chemical data to natural mantle fluids is supported by studies on major element solubility at high *P* and *T*. Experimental data up to 3 GPa and 1300°C indicate alkalis as the most soluble species in aqueous fluids, followed by Cl, Si, and Ca, while Mg and Fe are relatively less soluble (Brenan et al., 1995; Dvir et al., 2011; Eggler, 1987; Kawamoto et al., 2004; Manning, 2004; Nakamura and Kushiro, 1974; Newton and Manning, 2002; Stalder et al., 2001). For example, Nakamura and Kushiro (1974) estimated that 20 wt. % silica is dissolved in H_2O fluids coexisting with mantle enstatite at 1.5 GPa and 1280°C. The presence of CO_2 in the fluid strongly depresses the solubility of silica, while the presence of chlorine has the opposite effect (cf., Newton and Manning, 2010).

Previous direct measurements indicated that 10-14 wt% solutes (in NaCl equivalent) are present in hydrous fluid inclusions from the Ethiopian plateau (see section 2). Measured solute concentrations are in agreement with 2-5 wt% Cl (or 3.5-9 wt. % in NaCl equivalent) predicted for mantle fluids (Burgess and Turner, 1995), and with 6-10 wt % solutes measured in H_2O-rich subduction fluids (1-2 GPa; Manning, 2004). The total fluid solute content cannot have been extreme in order to trap homogeneous fluids in inclusions (Figs. 1 and 2). High-salinity aqueous fluids, having a large immiscibility solvus in the CO_2-H_2O-NaCl system, would have been immiscible with CO_2 at the considered mantle *P*-*T* conditions (Touret, 1992; 2009). Phase separation (into L+V) would have formed distinct CO_2-rich and saline-aqueous fluid inclusions in mantle minerals, which have not been observed. Based on these observations, the concentrated

449 brines (NaCl ≥ 50 wt %; Scambelluri et al., 1997) described in fluid inclusions of some
450 peridotites from subduction settings are likely to reflect the evolution of multicomponent fluids
451 towards increasing solute/H_2O ratios either by decompression-induced phase separation in the
452 CO_2-H_2O-salt fluid system, or by postentrapment inclusion "dehydration" trends.
453
454 *5.4 Origin of water and chlorine in shallow-mantle fluids*
455 Cl-bearing hydrous fluids may be common in subduction zones, generated by the breakdown
456 of hydrous minerals (e.g., serpentine; Manning, 2004; Poli and Schmidt, 2002; Scambelluri et
457 al., 2001; Sharp and Barnes, 2004). Thus, peridotites from mantle wedges are the best candidates
458 to find hydrous fluid inclusions. In this respect, fluid inclusions in peridotites from Central Italy
459 and Sardinia may testify to metasomatic fluids released during old subduction events. As noted
460 by Peccerillo (2005), in Italy and the southern Tyrrhenian sea, Plio-Quaternary magma
461 generation does not necessarily need to be coeval with subduction and mantle metasomatism; it
462 may postdate these processes, and could be triggered by changes in thermal regimes in the upper
463 mantle.
464 Our data raise the question of the origin of aqueo-carbonic fluids carrying significant amounts
465 of Cl in the lithosphere within the context of intraplate and extensional mantle settings (e.g.,
466 Ethiopia, and Hawaii) (Le Roux et al., 2006; Michael and Schilling, 1989; Seaman et al., 2004;
467 Stolper et al., 2004). In the east African lithosphere, evidence for mantle metasomatism driven
468 by Cl-bearing hydrous fluids is consistently reported from several xenolith localities and
469 supposed to have occurred during the early stages of mantle upwelling. The Cl-pargasite bearing
470 lithosphere under the Ethiopian plateau is considered to have been modally metasomatized by
471 CO_2-brine fluids, probably derived by degassing of deep carbonate rich melts during early stages
472 of upwelling of the Afar mantle zone (Frezzotti et al., 2010). Additionally, Cl-rich pargasite in
473 spinel lherzolites of Zabargad Island is interpreted to have formed just before the early rifting
474 phase of the Red Sea (Agrinier et al., 1993). In a similar way, the growth of amphibole ± Cl-

apatite in spinel peridotites from Yemen has been proposed to have been induced by the influx of carbonatitic melts and hydrous fluids from the Afar plume during the Oligocene (Baker et al., 1998). At Hawaii, Iceland, and Azores, Cl-enrichment in the lithosphere is indicated by the high Cl/F ratios of melt inclusions in OIB (e.g., Dixon et al., 2008; Le Roux et al., 2006; Michael and Schilling, 1989; Seaman et al., 2004; Stolper et al., 2004).

There should be other water and Cl-sources besides active subduction. Evidence for hydrous mantle fluids away from subduction zones has been obtained in cratonic areas by fluid inclusions in fibrous diamonds, where fluids consist of three main components: a carbonate melt, a silicate melt, and a hydro-saline fluid (e.g., Izraeli et al., 2001; Klein-BenDavid et al., 2004; 2007; Kopylova et al., 2010; Navon et al., 1988). The hydrous fluid component is enriched in SiO_2, Al_2O_3, halides, and alkalis (mainly K), similar to shallower hydrous fluids reported by this study. The total solute content is, however, considerably higher in diamond fluids (e.g., Cl up to ca. 35 wt. %), possibly reflecting the increase of elements solubility at greater *P* and *T* (*P* $\geq$ 4-5 GPa; e.g., supercritical fluid phases; Bureau and Keppler, 1999; Kawamoto et al., 2004; Kessel et al., 2005; Manning, 2004). In diamonds, continuous compositional variations of fluid inclusions are observed, suggesting that all components might be genetically related, most likely evolved from a "primitive" carbonate-rich melt (cf., Klein-BenDavid et al., 2004, and references therein). Recent experimental evidence shows that immiscibility processes in this silicate–carbonate–H_2O system facilitate the chlorine enrichment of the carbonate melt or of the aqueous fluid, not only at high pressures in the diamond stability field, but also at lithospheric pressures (Litasov and Ohtani, 2009; Litasov et al., 2011; Safonov, 2011).

It is conceivable to suppose that Cl-bearing hydrous shallow mantle fluids might have been formed through hydro-saline carbonate melts. As mentioned above, the model composition of hydrous shallow mantle fluids in spinel peridotites is similar to that of the aqueous fluid component trapped deeper, in diamonds. Further comparisons are difficult because of the limited data. Fluxes of CO_2-H_2O and Cl in the lithosphere could have been generated by degassing of

upwelling carbonate-rich melts at pressures below the carbonate-stability field (2–2.5 GPa; Dobson et al., 1996; Hammouda and Laporte, 2000). Since fluid data from mantle rocks in intraplate and extensional tectonic settings are limited, it is not known whether carbonate-melt degassing may be the main source of lithospheric hydrous fluids, or some other mechanisms, such as silicate melt – fluid immiscibility, have to be invoked. In any case, the deep association of CO_2, H_2O, carbonates, and diamonds preserved in fluid inclusions of Hawaiian garnet pyroxenites (Frezzotti an Peccerillo, 2007) was interpreted to have caught this process in the act.

6. Conclusions

The methodology presented in this paper shows that water is an elusive component in fluid inclusions in many hydrous and anhydrous upper mantle peridotites (i.e., Hawaii, Ethiopia, Canary Islands, and the western Mediterranean region). In shallow-mantle rocks, "pure CO_2" inclusions observed optically should be considered to contain less than 20 mole % of H_2O, in absence of spectroscopic analysis. Raman identification of H_2O, as OH^-, bound in hydrous silicates lining fluid inclusions suggests that hydrous fluid/host mineral chemical reactions represent a common postentrapment process, leading to fluid inclusion dehydration. FT-IR analysis of the distribution of water enrichment in mantle minerals suggests further dehydration through decrepitation, stretching, and H_2O diffusion.

Although shallow mantle fluids are generally dominated by CO_2, constraints from thermodynamic modeling in the MFSHC system suggest that up to 50 mole % H_2O could be present. Water activity (a_{H2O}) is expected to be low (probably < 0.4), in agreement with the anhydrous nature of many peridotite xenoliths. However, the existence of a hydrous fluid component will influence the physical and chemical evolution of the shallow mantle. Presence of H_2O and solutes makes migration of fluids more effective (Mibe et al., 1998, 1999; 2002; Watson and Brenan. 1987). Moreover, the solute content in such hydrous fluids will affect

transport and partitioning of elements inducing metasomatism in mantle rocks (Ayers, 1998; Keppler, 1996; Kessel at al., 2005; Konrad-Schmolke et al., 2011).

In extending present results to a broad statement about the composition of shallow-mantle fluid inclusions, we propose that multicomponent fluids are widespread in the shallow mantle, not only in subduction-zone settings, but also in extensional or intraplate settings. However, a stronger validation requires further spectroscopic (re)investigation of fluid inclusions in mantle peridotites.

Acknowledgments

We acknowledge T. Anderesen, J. Touret and an anonymous reviewer for most constructive reviews. We also thank B. Marty for his stimulating comments which greatly improved the manuscript. We are grateful to the National Museum of Natural History (Washington D.C.) for providing the Salt Lake Crater peridotite samples. We thank M. Placidi for the fine technical assistance on Raman spectroscopy, A. Perucchi for help in FT-IR maps treatment, as well as R. Bonelli and G. Giorgetti for help with SEM analyses. This study was supported by the Italian PRIN/2008BYTF98.

544 **References**

545 Agrinier, P., Mével, C., Bosch, D., Javoy, M., 1993. Metasomatic hydrous fluids in amphibole
546 peridotites from Zabargad Island (Red Sea). Earth Planet. Sci. Lett. 120, 187–205.
547 Andersen, T., Neumann, E.R., 2001. Fluid inclusions in mantle xenoliths. Lithos 55, 301-320.
548 Andersen T., O'Reilly, S.Y., Griffin W.L., 1984. The trapped fluid phase in upper mantle
549 xenoliths from Victoria. Implications for mantle metasomatism. Contrib. Mineral. Petrol. 88,
550 72-85.
551 Asimow, P.D., Langmuir, C.H., 2003. The importance of water to oceanic mantle melting
552 regimes. Nature 421, 815-820.
553 Aubaud C., Hauri, E.H., Hirschmann, M.M., 2004. Hydrogen partition coefficients between
554 nominally anhydrous minerals and basaltic melts. Geophys. Res. Lett. 31, L20611,
555 doi:10.1029/2004GL021341.
556 Ayers, J., 1998. Trace element modeling of aqueous fluid–peridotite interaction in the mantle
557 wedge of subduction zones. Contrib. Mineral. Petrol. 132, 390-404. Bailey, D.K., 1982.
558 Mantle metasomatism--Continuing chemical change within the Earth. Nature 296, 525-530.
559 Bailey, D.K., 1982. Mantle metasomatism: Continuing chemical change within the earth. Nature
560 296,525-530.
561 Baker, J.A., Chazot, C., Menzies, M., Thirwall, M., 1998. Metasomatism of the shallow mantle
562 beneath Yemen by the Afar plume: implications for plumes, flood volcanism, and intraplate
563 volcanism. Geology 26, 431–434.
564 Bakker, R.J., Jansen, J.B.H., 1991. Experimental post-entrapment water loss from synthetic CO_2-
565 H_2O inclusions in natural quartz. Geochim. Cosmochim. Acta 55, 2215-2230.
566 Bell, D.R., Ihinger, P.D., Rossman, G.R., 1995. Quantitative analysis of trace OH in garnet and
567 pyroxenes. Am. Mineral. 80, 465-474.
568 Bell, D.R., Rossman, G.R., Maldener, J., Endisch, D., Rauch, F., 2003. Hydroxide in olivine: a
569 quantitative determination of the absolute amount and calibration of the IR spectrum. J.
570 Geophys. Res. 108, 2105. doi:10.1029/2001JB000679.
571 Bolfan-Casanova, N., Keppler, H., Rubie, D.C., 2000. Water partitioning between nominally
572 anhydrous minerals in the MgO-SiO_2-H_2O system up to 24 GPa: implications for the
573 distribution of water in the Earth's mantle. Earth Planet. Sci. Lett. 182, 209-221.
574 Brenan, J.M., Shaw, H.F., Reyrson, F.J., Phinney, D.L., 1995. Mineral aqueous fluid partitioning
575 of trace elements at 900°C and 2.0 GPa: constraints on the trace element chemistry of
576 mantle and deep crustal fluids, Geochim. Cosmochim. Acta 59, 3331-3350.
577 Bureau, H., Keppler, H., 1999. Complete miscibility between silicate melts and hydrous fluids in
578 the upper mantle: experimental evidence and geochemical implications. Earth Planet. Sci.
579 Lett. 165, 187-196.
580 Burgess, R., Turner, G., 1995. Halogen geochemistry of mantle fluids in diamonds, in: Farley,
581 K.A. (Ed.), Volatiles in the Earth and Solar system. Proc. AIP Conf. 341, 91–98.
582 Clague, D.A., Frey, F.A., 1982. Petrology and trace element chemistry of the Honolulu
583 volcanics, Oahu: implication for the oceanic mantle below Hawaii, J. Petrol. 23, 447–504.
584 Connolly, J.A.D.,1990. Multivariable phase diagrams: an algorithm based on generalized
585 thermodynamics. Am. J. Sci. 290, 666-718.

586 Connolly, J.A.D., 1995. Phase-diagram methods for graphitic rocks and application to the system
587 C-O-H-FeO-TiO_2-SiO_2. Contrib. Mineral. Petrol. 119, 94-116.
588 Conticelli, S., 1998. The effect of crustal contamination on ultrapotassic magmas with lamproitic
589 affinity: mineralogical, geochemical and isotope data from the Torre Alfina lavas and
590 xenoliths, Central Italy. Chem. Geol. 149, 51-81.
591 Conticelli, S., Peccerillo, A., 1990. Petrological significance of high-pressure ultramafic
592 xenoliths from ultrapotassic rocks of Central Italy. Lithos 24, 305 - 322.
593 Dasgupta, R., Hirschmann, M.M., 2006. Melting in the Earth's deep upper mantle caused by
594 carbon dioxide. Nature 440, 659-662.
595 Demouchy, S., Jacobsen, S.D., Gaillard, F., Stern, C.R., 2006. Rapid magma ascent recorded by
596 water diffusion profiles in mantle olivine. Geology 34, 429-432.
597 Dixon, J.D.A., Clague, B., Cousens, M.L., Monsalve, Uhl, J., 2008, Carbonatite and silicate melt
598 metasomatism of the mantle surrounding the Hawaiian plume: Evidence from volatiles,
599 trace elements, and radiogenic isotopes in rejuvenated-stage lavas from Niihau, Hawaii,
600 Geochem. Geophys. Geosyst. 9, Q09005, doi:10.1029/2008GC002076.
601 Dixon, J.E., Dixon, T.H., Bell, D.R., Malservisi, R., 2004. Lateral variation in upper mantle
602 viscosity: role of water. Earth Planet. Sci. Lett. 222, 451–67
603 Dixon, J.E., Leist, L., Langmuir, C., Schilling, J.G., 2002. Recycled dehydratrated lithosphere
604 observed in plume-influenced mid-ocean-ridge basalt. Nature 420, 385-389.
605 Dobson, D.P., Jones, A.P., Rabe, R., Sekine, T., Kurita, K., Taniguchi, T., Kondo, T., Kato, T.,
606 Shimomura, O. and Urakawa, S., 1996. In-situ measurement of viscosity and density of
607 carbonate melts at high pressure. Earth Planet. Sci. Lett. 143, 207–215.
608 Dvir, O, Pettke, T., Fumagalli, P., Kessel, R., 2011. Fluids in the peridotite–water system up to 6
609 GPa and 800: new experimental constrains on dehydration reactions. Contrib. Mineral.
610 Petrol. 161, 829-844.
611 Eggler, D.H., 1987. Solubility of major and trace elements in mantle metasomatic fluids:
612 experimental constraints. In: Menzies MA, Hawkesworth CJ (eds) Mantle metasomatism.
613 Academic Press, New York, 21-42
614 Ferrando, S., Frezzotti, M.L., Neumann, E.R., De Astis, G., Peccerillo, A., Dereje, A., Gezahegn,
615 Y., Teklewold, A. 2008. Composition and thermal structure of the lithosphere beneath the
616 Ethiopian plateau: evidence from mantle xenoliths in basanites, Injibara, Lake Tana
617 Province. Mineral. Petrol. 93, 47-78.
618 Ferrando, S., Frezzotti, M.L., Petrelli, M., Compagnoni, R., 2009. Metasomatism of continental
619 crust during subduction: the UHP whiteschists from the Southern Dora-Maira Massif (Italian
620 Western Alps), J. Metamorphic Geol. 27, 739 – 756.
621 French, B.M., 1966. Some geological implications of equilibrium between graphite and a C-H-O
622 gas phase at high temperatures and pressures. Rev. Geophys. 4, 223-254.
623 Frezzotti, M.L., Peccerillo, A., 2007. Diamond-bearing COHS fluids in the mantle beneath
624 Hawaii. Earth Planet. Sci. Lett. 262, 273-283.
625 Frezzotti, M.L., Burke, E.A.J., De Vivo, B., Stefanini, B., Villa, I.M., 1992. Mantle fluids in
626 pyroxenite nodules from Salt Lake Crater (Oahu, Hawaii). Eur. J. Mineral. 4, 1137–1153.
627 Frezzotti, M.L., Andersen, T., Neumann, E.R, Simonsen, S.L., 2002a. Carbonatite melt-CO_2
628 fluid inclusions in mantle xenoliths from Tenerife, Canary Islands: a story of trapping,
629 immiscibility and fluid–rock interaction in the upper mantle. Lithos 64,77-96.

Frezzotti, M.L., Touret, J.L.R., Neumann, E.R., 2002b. Ephemeral carbonate melts in the upper mantle: carbonate–silicate immiscibility in microveins and inclusions within spinel peridotite xenoliths, La Gomera, Canary Islands. Eur. J. Mineral. 14, 891–904.

Frezzotti, M.L., Peccerillo, A., Panza, G., 2009. Carbonate metasomatism and CO2 lithosphere-astenosphere degassing beneath the Western Mediterranean: an integrated model arising from petrological and geophysical data. Chem. Geol. 262, 108-120.

Frezzotti, M.L., Ferrando, S., Peccerillo, A., Tecce, F., Petrelli, M., 2010. Chlorine-rich metasomatic H_2O-CO_2 fluids in amphibole-bearing peridotites from Injibara (Lake Tana region, Ethiopian plateau): nature and evolution of volatiles in the mantle of a region of continental flood basalts. Geochim. Cosmochim. Acta, 74, 3023 -3039.

Frezzotti, M.L., Tecce, F., Casagli, A., 2012. Raman spectroscopy for fluid inclusion analysis. J. Geochem. Expl. 112, 1-20.

Green, D.H., Falloon, T.J., 1998. Pyrolite: a Ringwood concept and its current expression. in Jackson, J. (Ed.), The Earth's Mantle. Cambridge Univ. Press, New York, pp. 311-378.

Grishina, S., Dubessy, J., Kontorovitch, A., Pironon, J., 1992. Inclusions in salt beds resulting from thermal metamorphism by dolerite sills (eastern Siberia, Russia). Eur. J. Mineral. 4, 1187-1202

Hammouda, T., Laporte, D. 2000. Ultrafast mantle impregnation by carbonatite melts. Geology 28, 283–285.

Hidas, K., Guzmics, T., Szabó, C., Kovács, I., Bodnar, R.J., Zajacz, Z., Nédli, Z., Vaccari, L., Perucchi, A., 2010. Coexisting silicate melt inclusions and H_2O-bearing, CO_2-rich fluid inclusions in mantle peridotite xenoliths from the Carpathian–Pannonian region (central Hungary). Chem. Geol. 274, 1-18.

Hirth, G., Kohlstedt, D.L., 2003. Rheology of the upper mantle and the mantle wedge: a view from the experimentalists, in: Eiler J. (Ed.), Inside the Subduction Factory. AGU, Washington, D.C., pp. 83–105.

Holland, T.J.B., Powell, R., 2011. An improved and extended internally consistent thermodynamic dataset for phases of petrological interest, involving a new equation of state for solids. J. metamorphic Geol. 29, 333-383.

Hollister, L.S., 1990. Enrichment of CO_2 in fluid inclusions in quartz by removal of H_2O during crystal-plastic deformation. J. Struct. Geol. 12, 895-901.

Huizenga, J.M., 2001. Thermodynamic modeling of C-O-H fluids. Lithos, 55. 101–114.

Huizenga, J.M., 2005. C-O-H, an Excel spreadsheet for composition calculations in the C-O-H fluid system. Comput. Geosci. 31, 797-800.

Jackson, E.D., Wright, T.L., 1970. Xenoliths in the Honolulu volcanic series, Hawaii, J. Petrol. 11, 405–430.

Izraeli, E.S., Harris, J.W., Navon, O., 2001. Brine inclusions in diamonds: a new upper mantle fluid. Earth Planet. Sci. Lett. 187, 323-332.

Katayama, I., Karato S.I., 2008. Low-temperature, high-stress deformation of olivine under water-saturated conditions. Phys. Earth Planet. Int. 168, 125-133.

Katz, R.F., Spiegelman, M., Langmuir, C.H., 2003. A new parameterisation of hydrous mantle melting. Geochem. Geophys. Geosyst. 4, 9, 1073.

Kawamoto, T., Matsukage, K.N., Mibe, K., Isshiki, M., Nishimura, K., Ishimatsu, N., Ono, S., 2004. Mg/Si ratios of aqueous fl uids coexisting with forsterite and enstatite based on the phase relations in the Mg_2SiO_4-SiO_2-H_2O system. Am. Mineral. 89,1433-1437.

675 Keppler H., 1996. Constraints from partitioning experiments on the composition of subduction-
676 zone fluids, Nature 380, 237-240.Keshav, S., Sen, G., 2001. Majoritic garnets in Hawaiian
677 xenoliths: preliminary results. Geophys. Res. Lett. 28, 3509-3512.
678 Keshav, S., Sen, G., 2003. A rare composite xenolith from Salt Lake Crater, Oahu: high-pressure
679 fractionation and implications for kimberlitic melts in the Hawaiian mantle. Contrib.
680 Mineral. Petrol. 144, 548-558.
681 Keshav, S., Sen, G., Presnall, D.C., 2007. Garnet-bearing xenoliths from Salt Lake Crater, Oahu,
682 Hawaii: High-pressure fractional crystallization in the oceanic mantle. J. Petrol. 48, 1681-
683 1724.
684 Kessel R., Schmidt M.W., Ulmer P., Pettke T., 2005. Trace element signature of subduction-
685 zone fluids, melts and supercritical liquids at 120-180 km depth, Nature, 437, 724-727.
686 Khisina, N.R., Wirth, R., Andrut, M., Ukhanov, AV., 2001. Extrinsic and intrinsic mode of
687 hydrogen occurrence in natural olivines: FTIR and TEM investigation. Phys. Chem. Miner.
688 28, 291-301.
689 Klein-BenDavid, O., Izraeli, E.S., Hauri, E., Navon O., 2004. Mantle fluid evolution – a tale of
690 one diamond. Lithos 77, 243–253.
691 Klein-BenDavid, O., Izraeli, E. S., Hauri, E., Navon, O., 2007. Fluid inclusions in diamonds
692 from the Diavik mine, Canada and the evolution of diamond-forming fluids. Geochim.
693 Cosmochim. Acta 71, 723–744.
694 Konrad-Schmolke, M., Zack, T., Brien, P.J., 2011. Fluid migration above a subducted slab:
695 thermodynamic and trace element modeling of fluid–rock interaction in partially overprinted
696 eclogite-facies rocks (Sesia Zone, Western Alps). Earth Planet. Sci. Lett. 311, 287-298.
697 Kopylova, M., Navon, O., Dubrovinsky, L., Khachatryan, G., 2010. Carbonatitic mineralogy of
698 natural diamond-forming fluids. Earth Planet. Sci. Lett. 291, 126-137.
699 Lamb, W.M., Valley J.W., Brown P.E., 1987. Post-metamorphic CO_2-rich fluid inclusions in
700 granulites. Contrib. Mineral. Petrol. 96, 485-495.
701 Lassiter, J.C., Hauri, E.H., Reiners, P., Garcia, M.O., 2000. Generation of Hawaiian post-
702 erosional lavas by melting of a mixed lherzolite/pyroxenite source. Earth Planet. Sci. Lett.
703 178, 269-284.
704 Le Roux, P.J., Shirey, S.B., Hauri, E.H., Perfit, M.R., Bender, J.F., 2006. The effects of variable
705 sources, processes and contaminants on the composition of northern EPR MORB (8–10°N
706 & 12–14°N): evidence from volatiles (H_2O, CO_2, S) and halogens (F, Cl). Earth Planet. Sci.
707 Lett. 251, 209–231.
708 Litasov, K.D., Othani, E., 2009. Phase relations in the peridotite–carbonate–chloride system at
709 7.0–16.5 GPa and the role of chlorides in the origin of kimberlite and diamond. Chem. Geol.
710 262, 29-41.
711 Litasov, K.D., Shatskij, A.F., Pokhilenko, N.P., 2011. Phase relations and melting in the systems
712 of peritotie-H2O-CO2 and eclogite-H2O-CO2 at pressures up to 27 GPa. Doklady Earth Sci.
713 437, 669-674.
714 Lustrino, M., Melluso, L., Morra, V., 2000. The role of lower continental crust and lithospheric
715 mantle in the genesis of Plio-Pleistocene volcanic rocks from Sardinia (Italy). Earth Planet.
716 Sci. Lett. 180, 259–270.
717 Lustrino, M., Brotzu, P., Lonis, R., Melluso, L., Morra, V., 2004. European subcontinental
718 mantle as revealed by Neogene volcanic rocks and mantle xenoliths of Sardinia. 32nd Int.
719 Geol. Congr., Post-Congress Guide P69, p. 42.

720 Luth, R.W., 2003. Mantle volatiles - distribution and consequences, in: Carlson, R. (Ed.) The
721 Mantle and Core, Volume 2, Holland, H.D., Turekian, K.K. (Eds.) Treatise on
722 Geochemistry. Elsevier-Pergamon, Oxford, pp. 319-361.
723 Mackwell, S.J., Kohlstedt, D.L., 1990. Diffusion of hydrogen in olivine: implications for water
724 in the mantle, J. Geophys. Res. 95, 5079-5088.
725 Manning, C.E., 2004. The chemistry of subduction-zone fluids. Earth Planet. Sci. Lett. 223, 1-
726 16.
727 Marty, B., Tolstikhin, I.N., 1998. CO_2 fluxes from mid-ocean ridges, arcs and plumes, Chemical
728 Geology, 145, 233-248.
729 Marty, B., Zimmermann L., 1999. Volatiles (He, C, N, Ar) in midocean ridge basalts:
730 Assessment of shallow-level fractionation and characterization of source composition,
731 Geochim. Cosmochim. Acta, 63, 3619-3633.
732 McInnes, B.I.A., Gregoire, M., Binns, R.A., Herzig, P.M., Hannington, M.D., 2001. Hydrous
733 metasomatism of oceanic sub-arc mantle, Lihir, Papua New Guinea; petrology and
734 geochemistry of fluid-metasomatised mantle wedge xenoliths. Earth Planet. Sci. Lett. 188,
735 169–183.
736 McMillan, P.F., Dubessy, J., Hemley, R., 1996. Raman Microscopy. Applications in Earth,
737 planetary and environmental sciences, in: Turrell, G., Corset, G. (Eds.), Academic Press, pp.
738 289–351.
739 Mibe, K., Fujii, T., Yasuda, A., 1998. Connectivity of aqueous fluid in the Earth's upper mantle.
740 Geophys. Res. Lett. 25, 1233-1236.
741 Mibe, K., Fujii, T., Yasuda, A., 1999. Control of the location of the volcanic front by aqueous
742 fluid connectivity in the mantle wedge. Nature 401, 259–262.
743 Mibe, K., Fujii, T., Yasuda, A., 2002. Composition of aqueous fluid coexisting with mantle
744 minerals at high pressure and its bearing on the differentiation of the Earth's mantle,
745 Geochim. Cosmochim. Acta 66, 2273– 2285.
746 Michael, P.J., Schilling J.-G., 1989. Chlorine in mid-ocean ridge magmas: evidence for
747 assimilation of seawater-influenced components. Geochim. Cosmochim. Acta 53, 3131–
748 3143.
749 Murck, B.W., Burruss, R.C., Hollister, L.S., 1978. Phase equilibria in fluid inclusions in
750 ultrarnafic xenoliths. Amer. Mineral. 63, 40-46.
751 Nakamura, Y., Kushiro I., 1974. Composition of the gas phase in Mg_2SiO_4-SiO_2-H_2O at 15 kbar,
752 in: Year Book Carnegie Inst. Wash. 73, pp. 255-258.
753 Navon, O., Hutcheon, I.D., Rossman, G.R., Wasserburg G.J., 1988. Mantle-derived fluids in
754 diamond micro-inclusions. Nature 335, 784–789.
755 Newton, R.C., Manning, C.E., 2002. Solubility of enstatite- forsterite in H_2O at deep crust/upper
756 mantle conditions: 4 to 15 kbar and 700 to 900°C. Geochim. Cosmochim. Acta 66, 4165-
757 4176.
758 Newton, R.C., Manning, C.E., 2010. Role of saline fluids in deep-crustal and upper-mantle
759 metasomatism: insight from experimental studies. Geofluids 10, 58-72.
760 Ohmoto, H., Kerrick, D., 1977. Devolatilization equilibria in graphitic systems. Am. J. Sci., 277
761 1013-1044.
762 Oppenheimer C., Moretti, R., Kyle, P.R., Eschenbacher, A., Lowenstern, J.B., Hervig, R.L.,
763 Dunbar, N.W., 2011. Mantle to surface degassing of alkalic magmas at Erebus volcano,
764 Antarctica. Earth Planet. Sci. Lett. 306, 261-271.

765 O'Reilly, S.Y., Griffin, W.L., 2000. Apatite in the mantle: implications for metasomatic
766 processes and high heat production in Phanerozoic mantle. Lithos 53, 217–232.
767 Pasteris, J.D., 1987. Fluid inclusions in mantle xenoliths, in: Nixon, P.H. (Ed.) Mantle Xenoliths.
768 Wiley, pp. 691-708.
769 Pasteris, J.D., Wanamaker, B .J., 1988. Laser Raman microprobe analysis of experimentally re-
770 equilibrated fluid inclusions in olivine: Some implications for mantle fluids. Am. Mineral.
771 13, 1074-l 088.
772 Paterson, M., 1982. The determination of hydroxyl by infrared absorption in quartz, silicate
773 glasses and similar materials. Bull. Mineral. 105, 20–29.
774 Patiño Douce, A.E., Roden, M.F., Chaumba, J., Fleisher, C., Yogodzinski, G., 2011.
775 Compositional variability of terrestrial mantle apatites, thermodynamic modeling of apatite
776 volatile contents, and the halogen and water budgets of planetary mantles. Lithos 14-31.
777 Philippot, P., Selverstone, J., 1991. Trace-element-rich brines in eclogitic veins: implications for
778 fluid composition and transport during subduction. Contrib. Mineral. Petrol. 106, 417-430.
779 Peccerillo, A., 2005. Plio-Quaternary volcanism in Italy. Petrology, geochemistry, geodynamics.
780 Springer, Heidelberg. 365 pp.
781 Pera, E., Mainprice, D., Burlini, L., 2003. Anisotropic seismic properties of the upper mantle
782 beneath the Torre Alfina area (northern Apennines, central Italy), Tectonophysics 370, 11–
783 30.
784 00175-6.
785 Poli, S., Schimidt, M.W., 2002. Petrology of subducted slabs. Ann. Rev. Earth Planet. Sci., 30,
786 207-235.
787 Roedder, E., 1965. Liquid CO_2 inclusions in olivine-bearing nodules and phenocrysts from
788 basalts. Amer. Mineral. 50, 1746-1782.
789 Roedder, E., 1972. Composition of fluid inclusions, in: Fleischer, M., (Ed.) Data of
790 Geochemistry, 6th edition, U.S. Geological Survey Professional Paper 440JJ.
791 Roedder, E., 1984. Fluid Inclusions. Mineral. Soc. America. Rev. Mineral. 12.
792 Romer, R.L., Franz, L., Wirth, R., 2006. Chemical and isotopic effects of retrogression in
793 metamorphic fluid inclusions. Contrib. Mineral. Petrol. 151, 174-186.
794 Safonov, O.G., 2011. Interaction of model peridotite with (Ca, Na_2)CO_3–KCl melts and H_2O-
795 KCl fluids at 1.0–2.5 GPa. Vestnik Otdelenia nauk o Zemle RAN, 3, NZ6086,
796 doi:10.2205/2011NZ000216.
797 Scambelluri, M., Piccardo, G.B., Philippot, P., Robbiano, A. and Negretti, L., 1997. High salinity
798 fluid inclusions formed from recycled seawater in deeply subducted alpine serpentinite.
799 Earth Planet. Sci. Lett. 148, 485-500.
800 Scambelluri, M., Bottazzi, P., Trommmmsdoff, V., Vannucci, R., Hermamann, J., Gòmez-
801 Pugnaire, M.T., Lòpez-Sànchez Vizcaino V., 2001. Incompatible element-rich fluids
802 released by antigorite breakdown in deeply subducted mantle. Earth Planet. Sci. Lett., 192,
803 457-470.
804 Seaman, C., Sherman, S.B., Garcia, M.O., Baker, M.B., Balta, B. Stolper, E., 2004. Volatiles in
805 glasses from the HSDP2 drill core. Geochem. Geophys. Geosyst. 5, Q09G16.
806 doi:10.1029/2003GC000596.
807 Sen, G., 1988. Petrogenesis of spinel lherzolite and pyroxenite suite xenoliths from the Koolau
808 shield, Oahu, Hawaii: implications for petrology of the post-eruptive lithosphere beneath
809 Oahu, Contrib. Mineral. Petrol. 100, 61–91.

Sharp, Z.D., Barnes, J.D., 2004. Water-soluble chlorides in massive seafloor serpentinites: a source of chloride in subduction zones. Earth Planet. Sci. Lett. 226, 243–254.

Shaw, C., 2009. Caught in the act - The first few hours of xenolith assimilation preserved in lavas of the Rockeskyllerkopf volcano, West Eifel, Germany. Lithos 112 , 511-523.

Shi, P.F., Saxena, S.K., 1992. Thermodynamic modeling of the C-H-O-S fluid system. Am. Mineral. 77, 1038-1049.

Smith, J.V., Delaney, J.S., Hervig, R.L., Dawson, J.B., 1981. F and Cl in the upper mantle: geochemical implication, Lithos 14, 133–147.

Stalder R., Ulmer, P., Thompson, A.B., and Gunther, D., 2001. High pressure fluids in the system MgO-SiO_2-H_2O under upper mantle conditions. Contrib. Mineral. Petrol. 140, 607–618.

Sterner, S.M., Bodnar, R.J., 1989. Synthetic fluid inclusions. VII. Re-equilibration of fluid inclusions in quartz during laboratory-simulated metamorphic burial and uplift. J. Metamorphic Geol. 7, 243-260.

Stolper, E., Sherman, S., Garcia, M.O., Baker, M.B., Seaman, C., 2004. Glass in the submarine section of the HSDP2 drill core, Hilo, Hawaii. Geochem. Geophys. Geosyst. 5, doi: 10.1029/2003GC000553.

Thompson, A.B., 1992. Water in the Earth's upper mantle. Nature 358, 295-302.

Touret, J.L.R., 1981. Fluids in metamorphic rocks. Chap. 8, in: Short Course in Fluid Inclusions: Application to Petrology. Miner. Assoc. Canada, Calgary, 6, pp. 182-208.

Touret, J.L.R., 1992. CO_2 transfer between the Upper Mantle and the atmosphere: temporary storage in the lower continental crust. Terra Nova 4, 87-98.

Touret, J.L.R., 2001. Fluids in metamorphic rocks. Lithos 55, 1-25.

Touret J.L.R., 2009. Mantle to lower-crust fluid/melt transfer through granulite metamorphism. Russian Geol. Geophys. 50, 1052-1062.

Trial, A.F., Rudnick, R.L., Ashwal, L.D., Henry, D.J., Bergman, S.C., 1984. Fluid inclusions in mantle xenoliths from Ichinomegata, Japan: Evidence for subducted H_2O. EOS Trans. Amer. Geophys. Union 65, 306.

Viti, C., Frezzotti, M.L., 2000. Re-equilibration of glass and CO_2 inclusions in xenolith olivine: a TEM study. Am. Mineral. 85, 1390-1396.

Viti, C., Frezzotti, M.L., 2001. Transmission electron microscopy applied to fluid inclusion investigations. Lithos 55, 125 - 138.

Wallace, P.J., 2003. From mantle to atmosphere: magma degassing, explosive eruptions, and volcanic volatile budgets. Developments in Volcanology, Volume 5, pp 105-127.

Watson, E.B., Brenan, J.M., 1987. Fluids in the lithosphere, 1. Experimentally determined wettening characteristics of CO_2–H_2O fluids and their implications for fluid transport, host-rock physical properties, and fluid inclusion formation. Earth Planet. Sci. Lett. 85, 497–515.

Wirth, R, Rocholl, A., 2003. Nanocrystalline diamond from the Earth's mantle underneath Hawaii. Earth Planet. Sci. Lett. 211, 357-369.

Wyllie, P.J., Ryabchikov, I.D., 2000. Volatile components, magmas, and critical fluids in upwelling mantle. J. Petrol. 41, 1195-1206.

Zhang, C., Duan, Z., 2009. A model for C–O–H fluid in the Earth's mantle. Geochim. Cosmochim. Acta 73, 2089-2102.

Zhang, C., Duan, Z., 2010. GFluid: An Excel spreadsheet for investigating C–O–H fluid composition under high temperatures and pressures. Comp. Geosc. 36, 569-572.

855
856
857 **Captions to Figures**

858

859 Fig. 1 - Raman detection of optically hidden liquid water in fluid inclusions. a) Trail of fluid
860 inclusions in orthopyroxene. White asterisks indicate those fluid inclusions where liquid H_2O
861 was detected by Raman spectroscopy. b) Raman spectrum of liquid H_2O rimming CO_2 in a fluid
862 inclusion in Fig. 2a.

863

864 Fig. 2 - Different extents of fluid inclusion-host reactions as detected by Raman
865 microspectroscopy. Inclusions show textural evidence for an increasing reaction degree with the
866 enclosing mineral going from microphotographs a-b, to c and d. a) Decrepitated high-density
867 (monophase) CO_2 fluid inclusion containing magnesite (Mgs) in orthopyroxene. b) Magnesite
868 (Mgs) and talc (Tlc) in apparently preserved high density (monophase) CO_2 fluid inclusions
869 distributed along a trail in olivine. c) Decrepitated and reacted fluid inclusion in olivine.
870 Inclusion contains two phase (liquid + vapor) CO_2, Mgs, and Tlc. d) Decrepitated and reacted
871 fluid inclusion in olivine. The inclusion is filled by aggregates of Tlc and Mgs, with no visible
872 fluid left. e) Raman modes of magnesite inside fluid inclusions. Unlabelled peaks refer to
873 enclosing olivine. f) OH^- Raman modes of talc recorded inside fluid inclusions.

874

875 Fig. 3 - EDS-EDAX and Raman analyses in open fluid inclusions. a) Electron microphotograph
876 of an open inclusion in olivine. Talc (Tlc) and magnesite (Mgs) coat the inclusionwalls. b)
877 Electron microphotograph of an open fluid inclusion in orthopyroxene. Tlc is distributed along
878 the inclusion walls. A thin microcrystalline coating of gypsum, KCl, NaCl, SiO_2, and Fe-Al
879 oxides is observed on talc crystals (inset). c) Qualitative EDS-EDAX chemical analysis of the
880 coating shown in Fig. 3b (inset image). d) Main Raman modes of gypsum inside the fluid
881 inclusion in Fig. 3b. Unlabelled peaks refer to enclosing orthopyroxene. e) OH^- Raman modes of

gypsum. Raman spectra in Fig. 3d and e were collected in the same area of EDS-EDAX analysis (inset image in 3b).

Fig. 4 - Association of fluid, and hydrous-silicate inclusions in clinopyroxene (Cpx) from hydrous peridotites. a) Photomicrograph showing trailbound fluid inclusions (f.i.) and pargasite (Prg) in Cpx in peridotites from Ethiopia. b) Photomicrograph showing trailbound fluid inclusions (f.i.) and phlogopite (Phl) in Cpx in peridotites from Sardinia. c) Back scattered electron image showing f.i. (black) and Prg (dark gray) distribution in Cpx. Spinel inclusions are also visible (white). Back scattered electron image image of f.i. (black) and Phl distribution in Cpx. Note that Phl and Prg inclusions have the same chemical composition as metasomatic phases in rocks.

Fig. 5 - Synchrotron FT-IR imaging of water distribution in orthopyroxene and garnet surrounding fluid inclusions. (a) Microphotograph showing fluid inclusion (f.i.) distribution in the investigated orthopyroxene area, plane polarized light. (b) Absorbance map in the 3000–3600 cm^{-1} region and calculated water contents in Opx (ppm). (c) Microphotograph of garnet containing fluid inclusions (f.i.), crossed polars. (e) Absorbance map in the 3000–3800 cm^{-1} region and relative calculated water contents in Grt (ppm). In FT-IR maps, the color scale is proportional to OH^- enrichment (increasing from blue to pink). Measured water contents are drawn with a precision of 20's of ppm. Ol = olivine; Spl = spinel.

Fig. 6 - Synchrotron FT-IR imaging of water distribution in olivine. Microphotograph of investigated area in olivine containing several fluid inclusions. b) Absorbance map in the 3000–3600 cm^{-1} region and calculated water contents in olivine (ppm). The color scale is proportional to OH^- enrichment (increasing from blue to pink). Measured water contents are drawn with a precision of 10's of ppm. c) Qualitative distribution map of OH absorbance for talc and

serpentine in the 3600–3800 cm^{-1} region, which allows to qualify hydrated phases in olivine. a.u.: arbitrary units.

Fig. 7 – *T*-X_{H2O} petrogenetic grids at 1.5 GPa, 1.0 GPa, 0.5 GPa, and 0.1 GPa in the MgO-FeO-SiO_2-H_2O-CO_2 system, calculated with En and Fo compositions at #mg = 0.9, calculated with the thermodynamic approach of Connolly (1990). White dots are the invariant points. Black solid curves highlight possible reactions between H_2O-CO_2 fluids trapped in inclusions and the surrounding magnesian orthopyroxene. All reaction equations are written such that the high-X_{CO2} assemblage is on the right side. The occurrence of talc as product of reactions depends on fluid pressure and on X_{H2O}(invariant point 1), see 5.2.

Fig. 8 - *P*-*T* petrogenetic grid at X_{H2O} = 0.3 in the MgO-FeO-SiO_2-H_2O-CO_2 system, calculated with En and Fo compositions at #mg = 0.9. White dots are the invariant points. Black thick solid curves highlight possible reactions between H_2O-CO_2 fluids trapped in inclusions and the surrounding orthopyroxene. All reaction equations are written such that the low-X_{H2O} assemblage is on the right side. The oval and the star indicate the *P*-*T* conditions of fluid inclusion trapping and fluid inclusion decrepitation, respectively. The thick black arrow (a) represents the *P*-*T* path of a mantle xenolith within the host lava. The dashed grey lines represent isochores of preserved (b), and decrepitated (c) fluid inclusions. The two thin black arrows represent the *P*-*T* paths of preserved (high density, isochore b), and decrepitated (low density, isochore c) fluid inclusions. As evident from the grid, syn-, and post-eruptive reactions between fluid inclusions and surrounding orthopyroxene can produce hydrous minerals (talc) only in low-density fluid inclusions (c).

***Highlights**

- Raman and FTIR in fluid inclusions can verify the hydrous nature of mantle fluids.
- Shallow mantle inclusions either contain H_2O or represent "dehydrated" fluids.
- Hydrous fluid inclusions carry significant amounts of Si, Cl, S, K, Ca, and Na.
- Solute-rich hydrous fluids may be widespread in the shallow mantle.

Figure 1

Click here to download Figure: Fig. 1.eps

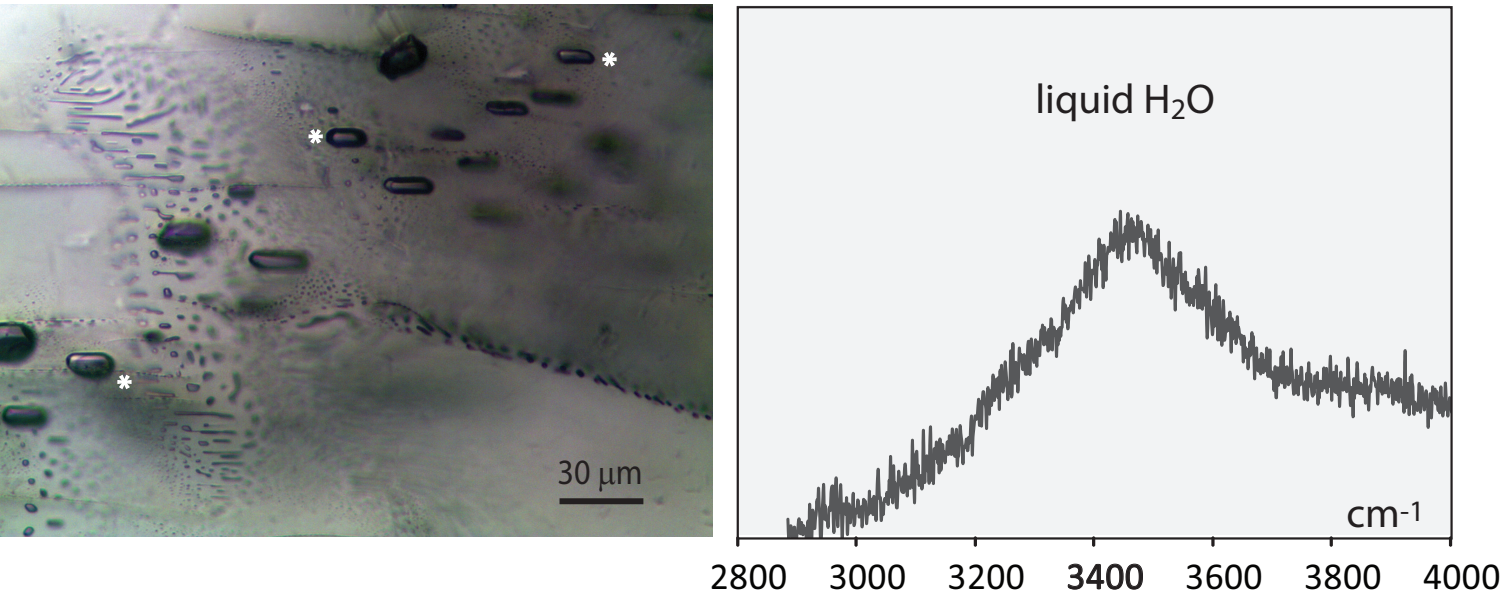

Figure 2

Click here to download Figure: Fig. 2.eps

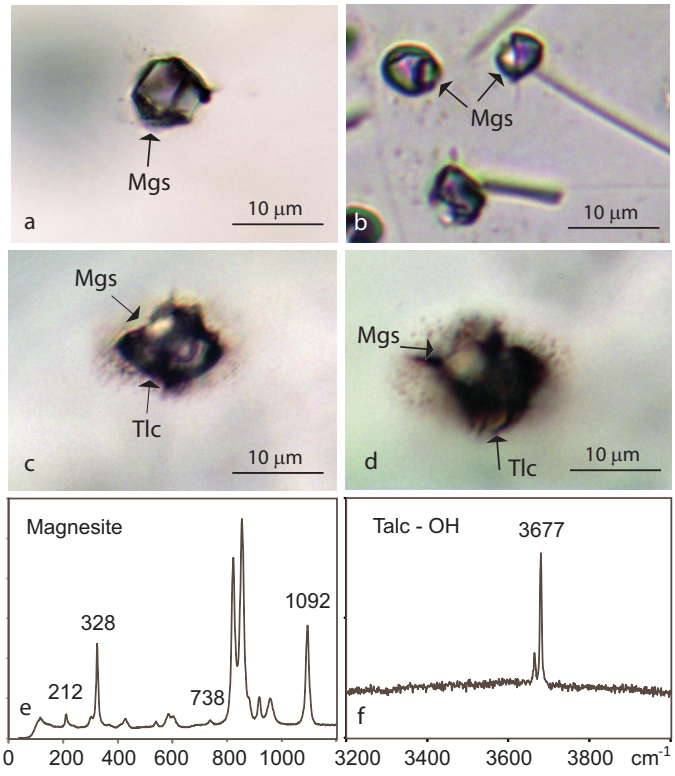

Figure 3

Click here to download Figure: Fig. 3.eps

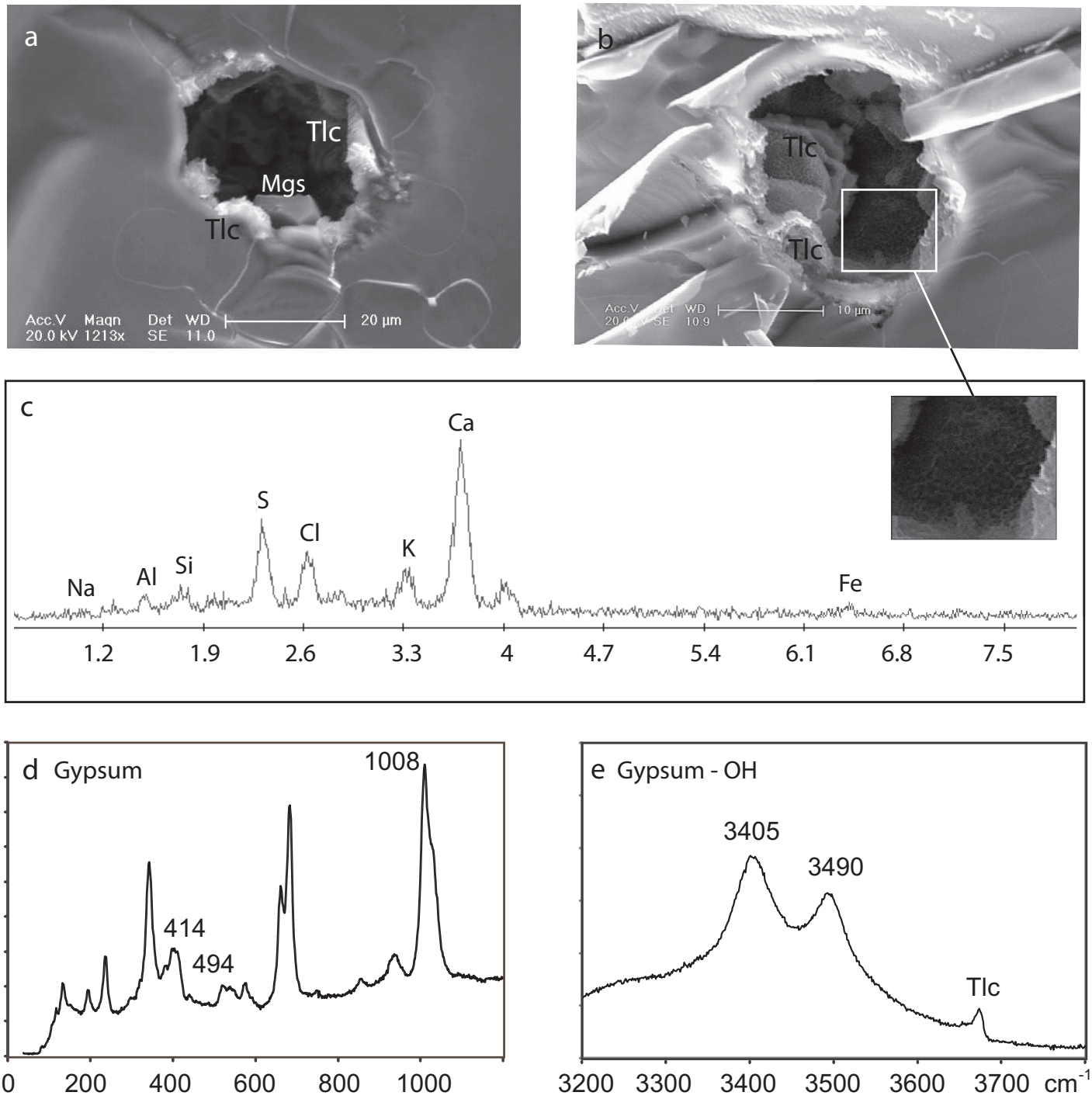

Figure 4

Click here to download Figure: Fig. 4.eps

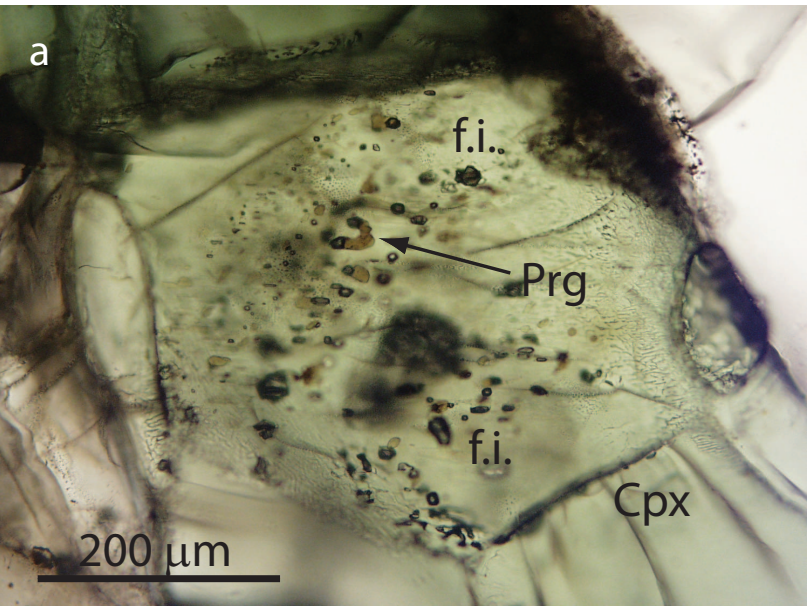

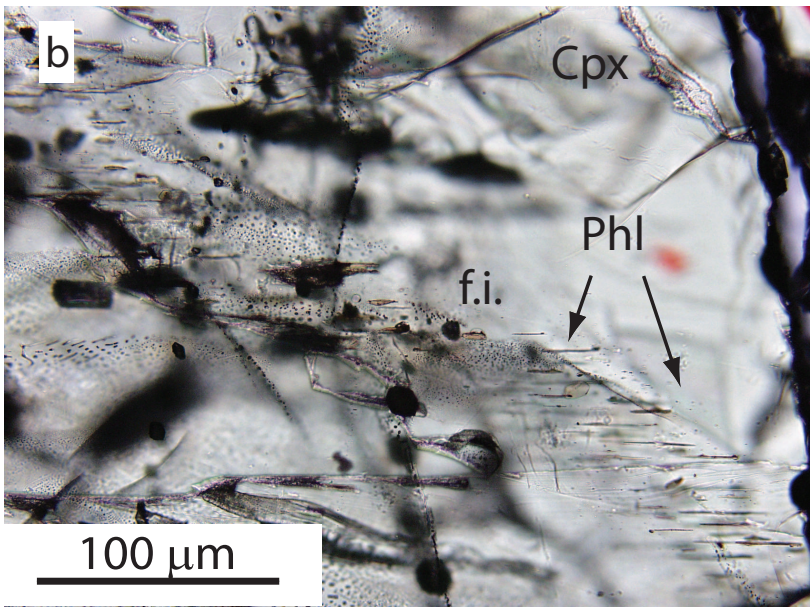

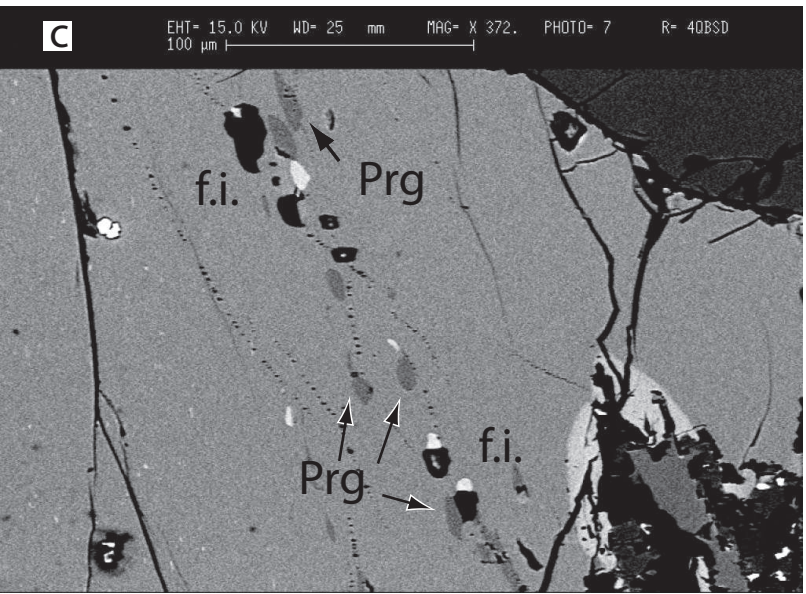

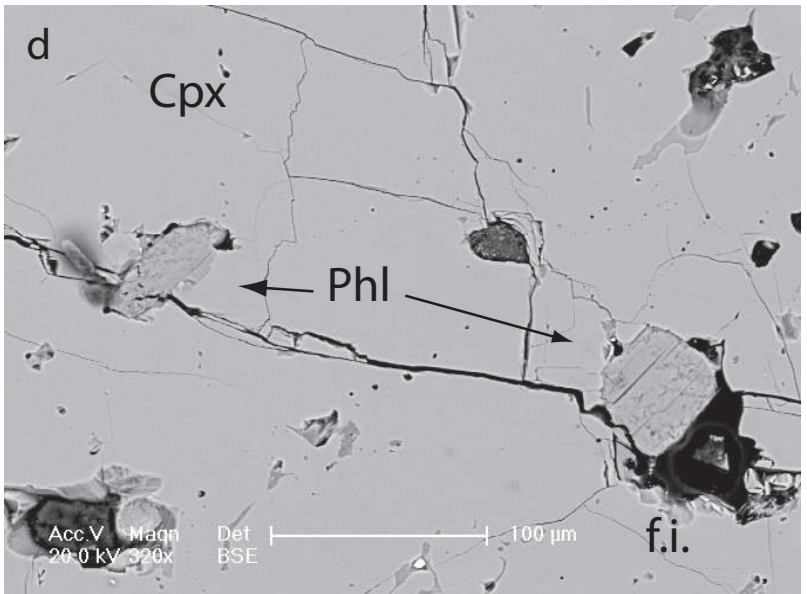

Figure 5

Click here to download Figure: Fig. 5.eps

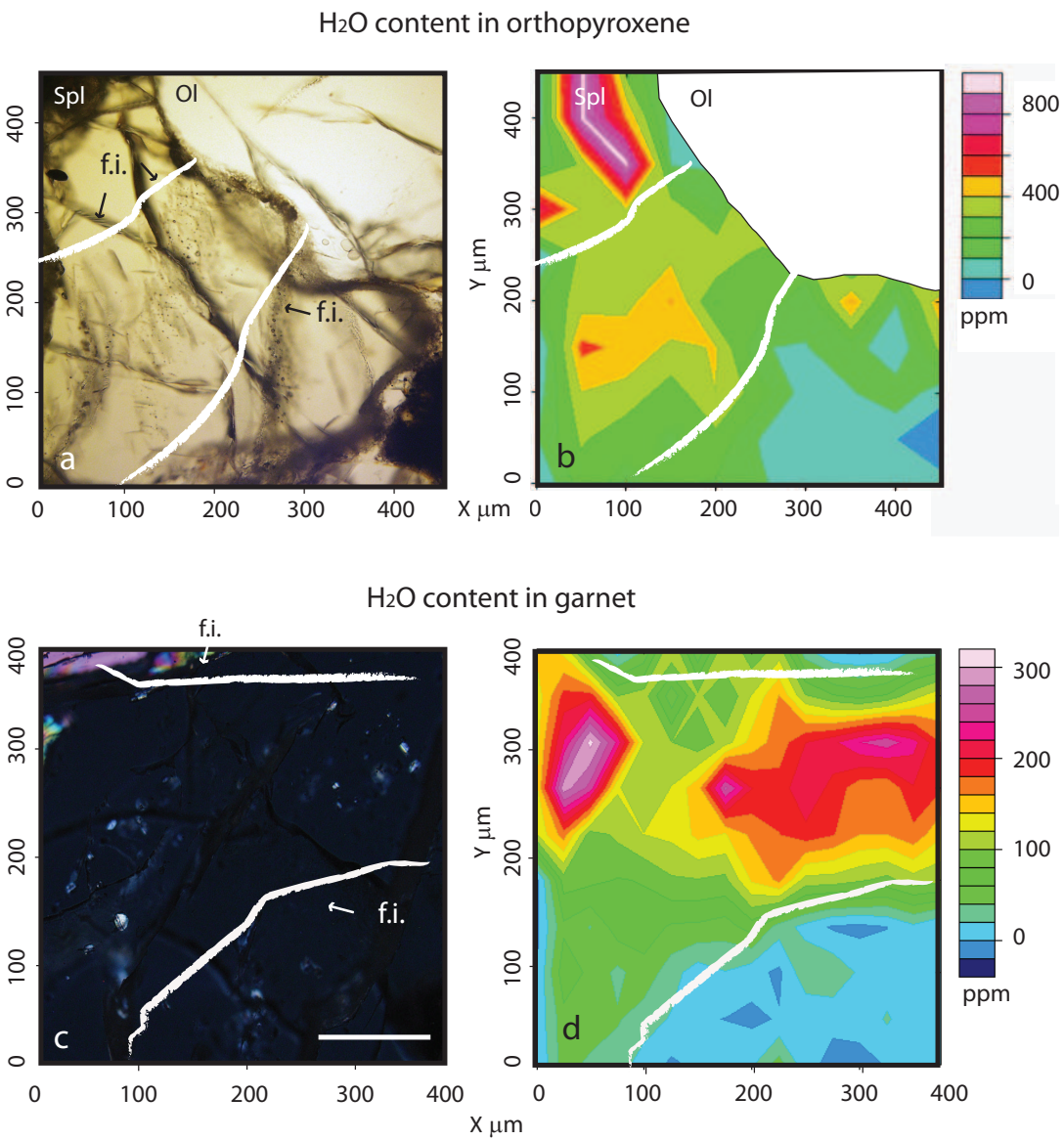

Figure 6
Click here to download Figure: Fig. 6.eps

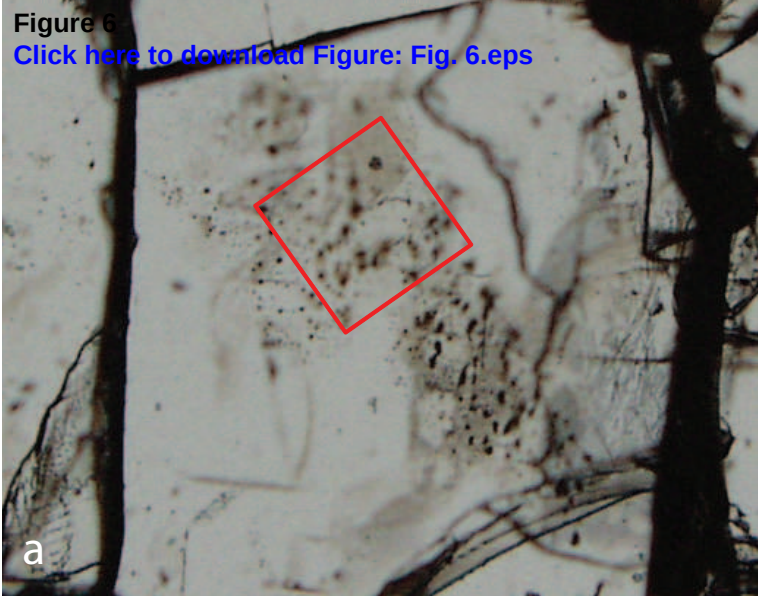

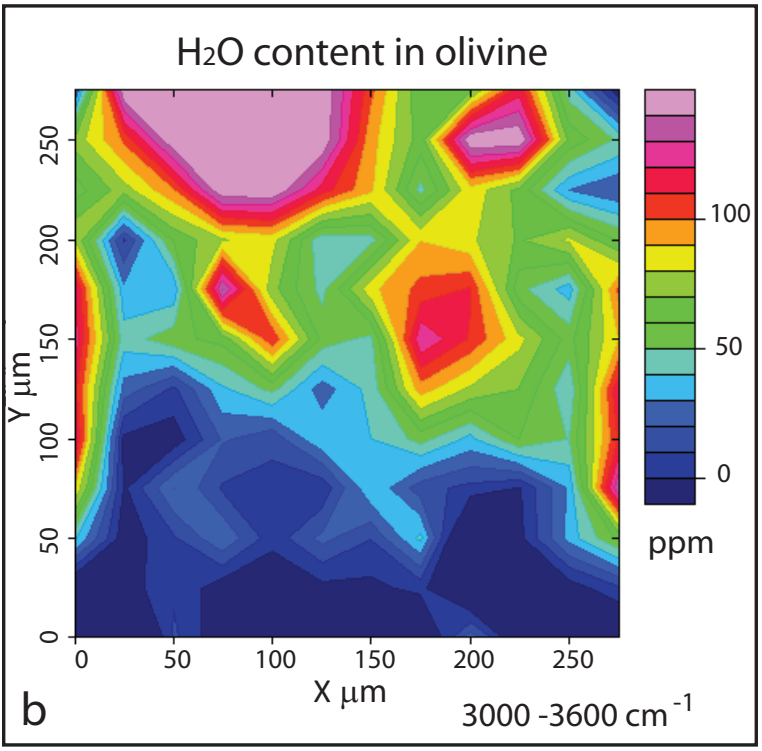

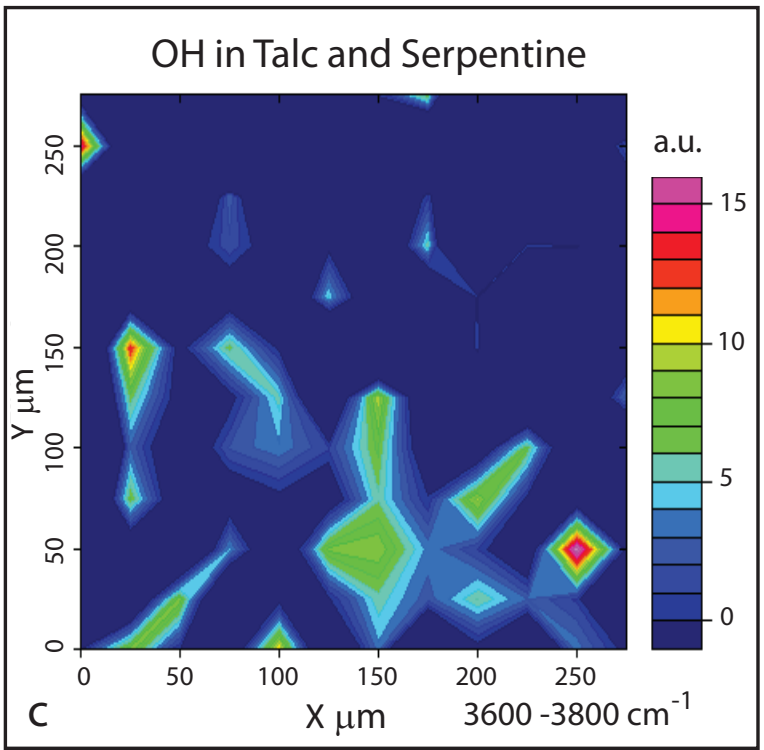

Figure 7

Click here to download Figure: Fig. 7.eps

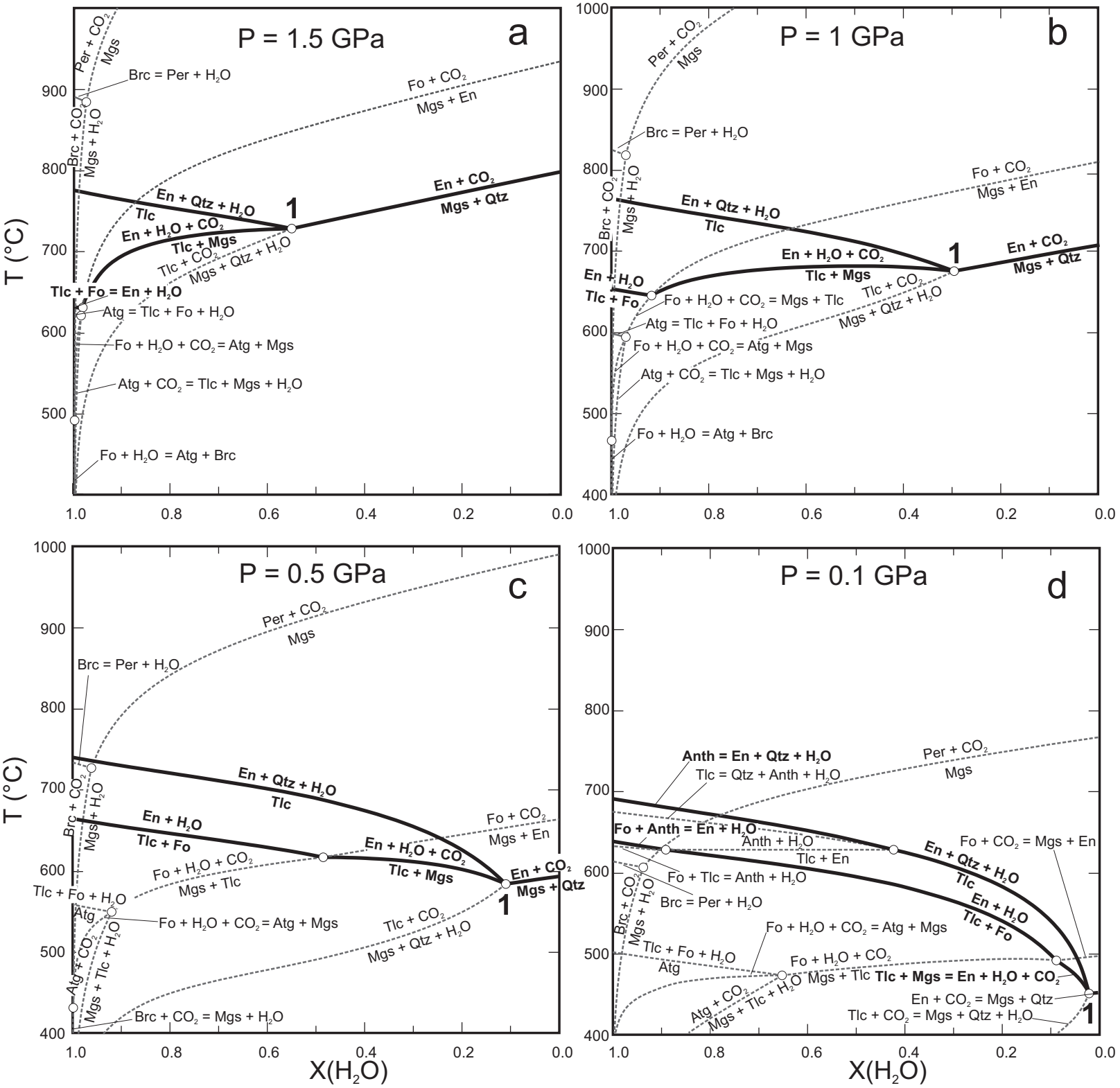

Figure 8

Click here to download Figure: Fig. 8.eps

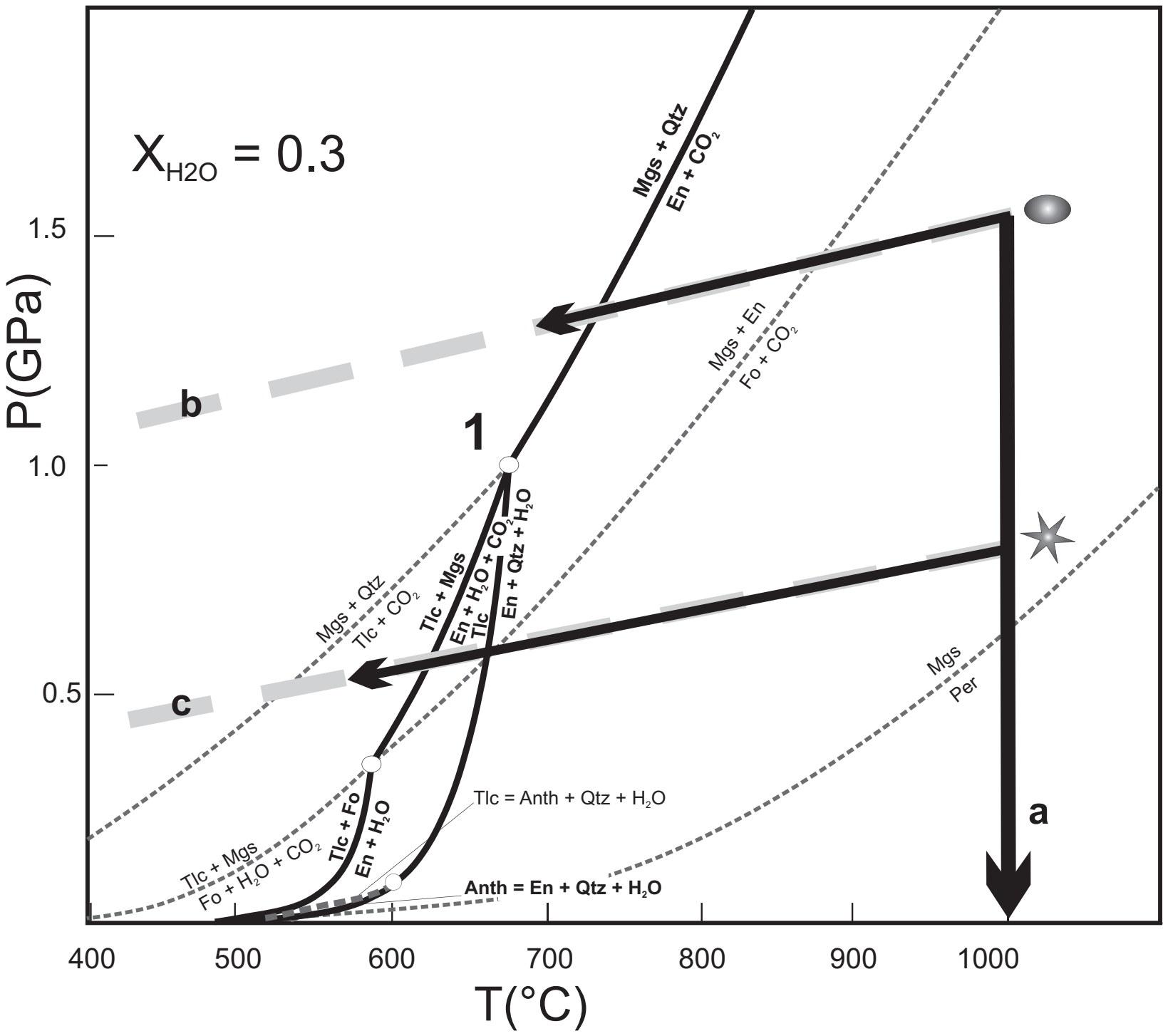

Table 1
Click here to download Table: Table 1.xlsx

Table 1 - Sample description

Peridotites						CO_2-rich fluid inclusions						
Locality	**Host rock**	**Rock type** (n° of samples)	**Texture**	**Mineralogy** (vol%)	***P-T* conditions**	**Host**	**Tm_{CO2}** (°C)	**ThL_{CO2}** (°C)	**$ThsL_{CO2}$** (°C)	**TsL_{CO2}** (°C)	**Tm_{Clat}** (°C)	***P* from isochores**
Hawaii Oahu, Salt Lake Crater	Honolulu volcanics: Alkali basalt, Basanite, Nephelinite lavas	Grt Pyroxenite (4)	granular	Ol (5-15) Opx (5-10) Cpx (65-85) Grt-Spl (1-6) Phl (0-traces)	1000 °C > 4.5 GPa	Ol Opx Cpx	-56.8/-56.6 -56.8/-56.6 -57/-56.6	-56.6/25 -56.6/24 -56.6/9.8	 -57.8/-56.6 -58.2/-56.7	 -57/-56.5 -57.9/-50.8		>1.8 GPa >1.8 GPa
Ethiopian volcanic plateau, Injibara	Basanite lavas	Spl Lherzolite (6)	protogranuar to porphyroclastic	Ol (50-70) Opx (20-30) Cpx (10-20) Spl (2-7) Prg (1)	950–1015 °C 1.3–2 GPa	Ol1 Opx1 Cpx	-57.6 / -56.5 -57.6 / -56.2 -57.9 / -56.3	-30.5 / 27.3 -39.2 / 30.9 -33.1 / 30.9			2.7 5.6	1.4–1.5 GPa
Italy Sardinia, Mt. Lisiri	Alkali basalt scoriae	Spl Pyroxenite (2)	granular	Ol (8-10) Opx (10-12) Cpx (80-85) Spl (1-4) Phl (1-2)	950-1050 °C 0.9-1.5 GPa	Ol Opx Cpx	-56.5 -56.8 / -56.6 -56.7 / -56.5	-13.8 / -4.8 -24 / 9.3 -14 / 29.3				0.95 GPa
		Spl Dunite (3)	porphyroclastic	Ol (90-95) Opx (<1) Cpx (1-6) Spl (1-3)		Opx1 Cpx	-56.6 -57 / -56.6	-11.7 / 3 -27.3 / 26.1				1 GPa
Central Italy Torre Alfina	Lamproite lavas	Spl Harzburgite, Spl Dunite (3+1)	protogranular	Ol (80-95) Opx (3-12) Cpx (1-4) Spl (1-4) Phl (1-10)	950-1080 °C 1.2-1.6 GPa	Opx1	-	-				1.2 GPa*

Ol = Olivine; Opx = Orthopyroxene; Cpx = Clinopyroxene; Spl = Spinel; Grt = Garnet; Prg = Pargasite; Phl = Phlogopite; Tm = temperature of melting; ThL = temperature of homogenization to liquid; ThsL = temperature of homogenization to liquid in presence of solid CO2 - superdense CO2 inclusions; TsL= temperature of solid CO2 final melting - superdense CO2 inclusions; Hhl = hydrohalite; Clat = clathrate; Ol1, Opx1 = olivine and orthpyroxene porphyroclasts; * Pressures derived from Raman CO2 density data (cf., Frezzotti et al., 2012).

Table 2
Click here to download Table: Table 2.xlsx

Table 2 - Detection of water and solutes in fluid inclusions in mantle mineral using different analytical techniques

Mantle Rocks				**Water and solutes in individual fluid inclusions**					
Locality	**Rock type**	**Hydrous Minerals**	**Host Mineral**	**Analytical technique**					**Fluid composition**
				Microsc.	Microther.	Raman	FT-IR	EDS Microprobe	
Canary*	Sp Lherz.	No	Ol	No	No	Talc - Magnesite	-	Talc - NaCl	CO_2
	Sp Harz.		Opx	No	No	-	-	No	+
			Cpx	No	No	-	-	No	H_2O, SiO_2 and NaCl
Hawaii	Grt Pyrox.	No	Ol	No	No	H_2O - CO_2	-	No	CO_2 (Carbonate melt)
			Opx	No	No	H_2O - CO_2	-	-	+
			Cpx	No	No	H_2O - CO_2	-	No	H_2O, H_2S and N_2
			Grt	No	No	No	-	-	
Ethiopia	Sp Lherz.	Prg	Ol	No	No	Talc/Clinochlore (rare) Magnesite - H_2O - CO_2	H_2O - OH^-	Magnesite - Talc	CO_2
			Opx	Yes	Yes	H_2O - CO_2	H_2O	-	+
			Cpx	No	No	-	No	-	H_2O, SiO_2, KCl and NaCl
Sardinia	Sp Pyrox.	Phl	Ol	No	No	Talc - Magnesite	-	K, Cl, S, Ca, Na	CO_2
	Sp Dun.		Opx	No	No	Talc (rare) - Magnesite	-	K, Cl, S, Ca, Na	+
			Cpx	No	No	Gypsum (rare) Dolomite - Talc (rare)	-	-	H_2O, SiO_2, KCl, NaCl, $CaSO_4$
Central	Sp Harz.	Phl	Opx	No	No	H_2O - CO_2 - S_8	-	-	CO_2 + H_2O and S
Italy	Sp Dun.		Cpx	No	No	No	-	-	

Ol = Olivine; Opx = Orthopyroxene; Cpx = Clinopyroxene; Sp = Spinel; Grt = Garnet; Prg = Pargasite; Phl = Phlogopite; Lherz. = Lherzolite; Harz. = Harzburgite; Dun. = Dunite; Pyrox. = Pyroxenite; f.i. = Fluid inclusions; Microsc. = Microscopy; Microther. = Microthermometry; - = not analyzed. * data from Frezzotti et al., 2002a.